10-2003

Corrosion and mass transport processes in Carbon steel miniature waste packages

James Cizdziel

Kaveh Zarrabi
Community College of Southern Nevada

Susan LeStrange
University of Nevada, Las Vegas

Amy J. Smiecinski
University of Nevada, Las Vegas, smiecins@unlv.nevada.edu

CORROSION AND MASS TRANSPORT PROCESSES IN CARBON STEEL MINIATURE WASTE PACKAGES

Dr. Kaveh Zarrabi
Department of Physical Sciences
Community College of Southern Nevada
Las Vegas, Nevada

Susan McMillan and Sandra Elkonz
Undergraduate Research Students
Department of Chemistry
University of Nevada, Las Vegas
Las Vegas, Nevada

Dr. James Cizdziel
Harry Reid Center for Environmental Studies
University of Nevada, Las Vegas
Las Vegas, Nevada

Document TR-03-003, Revision 0
Prepared for the U.S. DOE/UCCSN Cooperative Agreement
Number DE-FC08-98NV12081

Task 34

Originator:
Dr. James Cizdziel [redacted] Date 10-3-03

Principal Investigator:
Dr. Kaveh Zarrabi [redacted] Date 10-2-03

Technical Reviewer:
Dr. Susan LeStrange [redacted] Date 10-16-03

QA Reviewer:
Amy Smiecinski [redacted] Date 10-17-03

Acknowledgments

We would like to thank Susan LeStrange and Amy Smiecinski for many helpful suggestions and comments on our report. We also like to thank the U.S. Department of Energy for funding this research through Cooperative Agreement, DE-FC28-98NV12081, Task 34.

Summary

In this study, we have systematically investigated corrosion and mass transport processes in carbon steel miniature waste packages (MWP) in dynamic systems (water in, water out) under varying chemical conditions. The MWP were fabricated to have similar configuration to the DOE Spent Nuclear Fuel (SNF) waste package and that individual components to be in scale with each other compare to the SNF waste package. Two MWP configurations were studied: a "bathtub" model and a "flow-through" model. By slowly dripping 4 different solutions (groundwater obtained from well water J-13 located near Yucca Mountain, and J-13 water adjusted to low-pH, high-salinity, and high salinity-high nitrate) into the MWP, we were able to investigate the manner of oxidation, identify transported minerals contained in the effluent, and characterize the mass transport in terms of particle size.

Manner of oxidation. Through time-lapse digital photography, we were able to document the process of corrosion within a glass walled MWP. Formation of colored corrosion products including short-lived colored complexes was noted. A sequence of possible corrosion products was proposed. The availability of oxygen and limitation of diffusion through corrosion products lowers the rate of the corrosion process. In most cases the MWP exit hole sealed within 4 weeks of water introduction, resulting in overflow from the top of the MWP. This self-sealing is likely due to the larger molar volume of the corrosion products. The overflow water traveled on the outer surface of the MWP and hung at bottom before dripping out. Under these conditions corrosion to the bottom of the MWP was observed and eventual bottom failure is likely. It is recommended an addition of a skirt to the actual waste packages to deflect water away from the waste package.

Identification of Transported Minerals. Through X-Ray Diffraction and Scanning Electron Microscopy studies of solids in the MWP effluent, we discovered that secondary minerals, such as goethite were prevalent. Many of these corrosion products were amorphous and would expect to have different properties (buffering, sorption) compared to more crystalline minerals. Individual particles ranged from about 0.2 to 0.8 μm in diameter and larger conglomerates of particles up to several μm in diameter were also present.

Mass Transport of Solids. The greatest mass of solids transported out of the MWP occurred under acidic conditions followed by the control (J-13) solution. The salt (high ionic strength) solutions were more variable due to experimental difficulties but appear not to enhance the corrosion process. The nature of the transported material also differed by solution-type. As expected, most of the iron (>80%) was found in the dissolved state under acidic conditions, while solids (>0.45μm in diameter) dominated in the effluent of the other solutions.

TABLE OF CONTENTS

LIST OF FIGURES

LIST OF TABLES

KEY FOR SELECT ABBREVIATIONS

BN = Bathtub with No-shot
FN = Flow-through with No-shot
BI = Bathtub with Iron-shot
FI = Flow-through with Iron-shot
HS = High Salt
LPH = Low pH
HS-HN= High Salt – High Nitrate
C = "Control" (J13 well water)
25 = 25°C
80 = 80°C

UCCSN DATA ID TRACKING NUMBERS

034JC.001 Changes of pH, Conductivity, and Dissolved Oxygen in effluent solution during Miniature Waste Package Corrosion

034JC.002 Mass Transport of solids in effluent solution during Miniature Waste Package Corrosion

034JC.003 Graphical X-Ray Diffractometer Data and Mineral Analysis of Filtered Solids from effluent solution during Miniature Waste Package Corrosion.

034JC.004 Mass Transport of solids in effluent solution during Miniature Waste Package Corrosion: Second Experimental Run

034JC.005 Changes of pH, Conductivity, and Dissolved Oxygen in effluent solution during Miniature Waste Package Corrosion: Second Experimental Run

034JC.006 Concentration of dissolved iron in effluent solution from Miniature Waste Package Corrosion Study by ICPMS

034JC.007 ICPMS weight data for iron concentration calculations and report figures and tables

1. Introduction

The potential Monitored Geologic Repository is a system under study for disposal of spent nuclear fuel (SNF) at the proposed Yucca Mountain, Nevada site. Contact of groundwater with the waste package over time (hundreds or thousands of years) could initiate corrosion and possible losses of structural materials, neutron absorbers, and fuel materials. In this study, we designed and fabricated a replica miniature waste package (MWP) composed entirely of carbon steel, and introduced groundwater collected from well J-13 (located near Yucca Mountain), as well as J-13 groundwater adjusted to low pH, high saline, and high saline and nitrate conditions. The purpose was to evaluate corrosion and mass transport processes in a dynamic system under varying chemical conditions and experimental parameters. A schematic of the experiment is given in Fig. 1.

Figure 1. Schematic of Miniature Waste Package Experiment

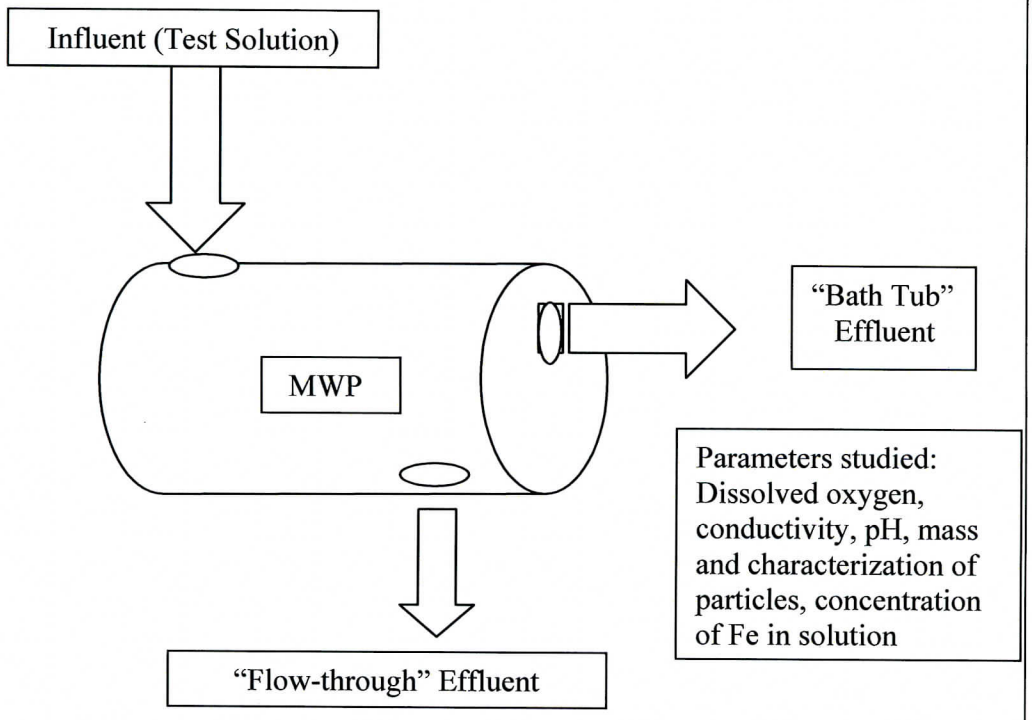

While the major structural material of the actual SNF waste package is stainless steel and alloys (Composition in Table 1), we have employed carbon steel to speed the corrosion process. The oxidation products of carbon steel may include a variety of minerals such as hematite (Fe_2O_3), goethite (FeOOH), and magnetite (Fe_3O_4). The newly formed minerals could potentially influence the waste package by slowing down the flow of groundwater

and thus influence the extent of oxidation. They may also be transported by groundwater flow outside the waste package, possibly as colloidal particles. If these processes continue without sealing the waste package, then, over the years large amounts of the steel could convert to corrosion products and leave the waste package. The volume of corrosion products will be replaced with groundwater, which may act as a neutron moderator and increase the likelihood of criticality within the package.

Table 1. Typical composition (Wt %) of some potential waste package materials[1]

Element	A516 Carbon Steel	304L Stainless Steel	316L Stainless Steel	C22-Alloy
Carbon	0.30	0.03	0.03	0.015
Manganese	1.025	2.00	2.0	0.50
Phosphorous	0.035	0.045	0.045	0.02
Sulfur	0.035	0.03	0.03	0.02
Silicon	0.275	0.75	0.75	0.08
Chromium	-	19.0	17.0	21.25
Nickel	-	10.0	12.0	54.765
Molybdenum	-	-	2.5	13.5
Nitrogen	-	0.1	0.1	-
Iron	98.33	68.045	65.545	4.0
Cobalt	-	-	-	2.5
Tungsten	-	-	-	3.0
Vanadium	-	-	-	0.35

[1] CRWMS M&O (1999). Non-Q, for information only.

In addition, water may gradually dissolve the fissile components and neutron absorbers and transport them outside the waste package as solutes or adsorbed species on colloidal iron oxyhydroxide particles. The formation of iron oxyhydroxide may also reduce the void volume within the waste package due to its larger molar volume and low solubility compared with iron. Such a scenario is supported by the existence of natural analogs in the environment (e.g., buried nails and sunken ships). If, however, iron oxyhydroxides are removed or solubilized, the waste package may require the addition of more neutron absorbers like B_4C control rods or Alloy 22 with gadolinium. Therefore, it is important to identify oxidation patterns of steel components within the waste package, and to identify and quantify the amounts of solid materials that could be transported out. To that end, the primary objectives of this study were to: (1) evaluate the "manner of oxidation" in the MWP under varying conditions of pH and conductivity, (2) identify formed

minerals, and (3) measure the amount of material transported by water flowing out of the MWP.

2. Experimental Design

In designing this study it was evident that variability of the system could influence experimental results. The main source of systematic errors was from operation of analytical instruments. The random errors could be variation in the pumping of test solutions. Existence of dynamic conditions inside the MWP could effect entrainment or settling of corrosion particles inside MWP. In addition, existence of preferential pathways for incoming water traveling through MWP contributes to differences in rate of corrosion and transport of solids from MWP.

Table 2 is the basic matrix representing samples that were analyzed in this study (EXP I). However, a concern was raised on efficiency of "washing" process in removing salts that could have been recrystallized on the papers. As a result, EXP I was repeated (EXP II) on selected samples contained high concentration of salts. Both sets of data are presented in this report. However, for "high salt" samples, results from EXP II were used in discussions. Drip rates onto the MWP were selected to be as close to those expected at Yucca Mountain. The estimates of water drip rates that are expected to enter the drift were obtained from a study (BSC 2003) where moderate rate was 0.015 m^3/year and high rate was 0.15 m^3/year.

Both "Bath Tub" and "Flow-through" experiments have a similar setup, except the location of the water exit hole. Three sets of experiments were conducted with each MWP. In one set of experiments the pH of the water inflow was changed to simulate pH changes that could occur due to dissolution of glass in DOE's Glass Pour Canisters (GPC) and Stainless Steel components of the waste packages. In the next set of experiments, saline J-13 well water was used to simulate saline seepage water. The last set of experiments simulated waste packages with or without iron shot (used to reduce void volume in the WP). Table 2 is a summary of experiments that were performed for each model. Each experiment was conducted at 25°C, except for a few select experiments at 80°C. The experiments were continued until transport of solids ceased or achieved a steady state.

Table 2: Experimental Matrix for "Bath Tub" and "Flow-through" Models for 25°C and 80°C

Water Flow pH Characteristics*	MWP
J-13 Well Water (Control)	No Iron shot
J-13 Well Water (Control)	With Iron shot
Low pH, J-13 Well Water	No Iron shot
Low pH, J-13 Well Water	With Iron shot
High Salt J-13 Well Water	No Iron shot
High Salt J-13 Well Water	With Iron shot
High Salt-High Nitrate J-13 Well Water	No Iron shot
High Salt-High Nitrate J-13 Well Water	With Iron shot

3. Materials and Methods

3.1 Selection and Preparation of Test Solutions

An important factor in assessing the performance and safety of the potential nuclear waste repository at Yucca Mountain is the composition of drift water that might seep onto waste packages over time and initiate corrosion and mass transport. We have selected four different solutions to introduce to our MWP based on possible chemical scenarios that could be encountered within a breached waste package and to evaluate the effects of high salt, high salt-high nitrate, and low pH on potential corrosion and tranport processes.

J-13 Well Water (Control Solution). J-13 is a well located near Yucca Mountain. Groundwater from this well was selected because it is commonly used as a reference water in the Yucca Mountain Project. Groundwater was collected after pumping three well-volumes and after stabilization of pH and conductivity was achieved. Water from this well has been collected and analyzed periodically over the last two decades and its composition (Table 3) has been stable over this span (CRWMS M&O 2000a). For this study, the water was collected into 10 L polypropylene containers and transported with ice in coolers to the laboratory. There it was stored at 4°C until the start of the experiment. The water was used unaltered as the "control" solution and to prepare the other test solutions (below) (I = 0.00249).

Table 3. Composition of J-13 Well Water[1]	
Component	**Concentration[2]**
Na^+	45.8
K^+	5.04
Ca^{++}	13.0
Mg^{++}	2.01
NO_3^-	8.78
Cl^-	7.14
F^-	2.18
SO_4^{2-}	18.4
Si	28.5
PO_4^{3-}	0.12
Alkalinity[3]	128.9
PH	7.41

[1] CRWMS M&O (2000a). Non-Q, for corroborative use only.
[2] mg/l, except for pH and alkalinity.
[3] mg/HCO_3^-.

High Saline Solution: Solutions with high salt content have been shown to enhance corrosion (Trefz et al. 1996). Salts, mostly chlorides, are expected to be present in pores at the repository site when heat generated from waste packages drives off pore water early in the life of repository. As the repository environment cools, condensed water can redissolve salt remaining in the pores. This will result in formation of a relatively saline solution that can come in contact with the waste package. Our high saline test solution was prepared, in part, based on information from Rosenberg et al. (1999) who reported on the evaporative chemical evolution of synthetic J-13 water. It was prepared by adding NaCl (100.8857 g), $NaHCO_3$ (433.8497 g), NaF (33.5978 g), KNO_3 (109.7600), and Na_2SO_4 (232.1714 g) to 10 L of J-13 water and stirring until fully dissolved. Each salt was reagent grade and obtained from JT Baker (I = 1.3705).

Low pH: Low pH is relevant because hydrogen ion can be generated by hydrolysis of some brine components and steels. Low pH conditions could occur in the repository environment due to a variety of scenarios. Many simulation studies on criticality and in-package chemistry show corrosion of carbon and stainless steel to cause the pH of the solution to drop. Dissolution of the Department of Energy's Glass Pour Canisters, and

corrosion of the C22 alloy and stainless steel components of the waste packages, which contain significant amounts of chromium and molybdenum, could produce more acid, per volume, than carbon steel alone (CRWMS M&O 2000c). Thus, the low pH test solution was selected to mimic time periods in the corrosion process in which low pH is expected to be encountered. For this study, the low pH solution was prepared by adding 10 mL of ultra pure nitric acid (Ultrex II; JT Baker; Lot #H51548) to 10 L of J-13 well water. The pH of the resulting solution was 1.89 (I = 0.00223).

High Saline – High Nitrate: A high salt-high nitrate solution was selected to include the possibilty of additional formation of nitrate due to radiolysis inside the waste package. In such a solution nitrate ions may play a more important role in the corrosion process than other anions. The high saline – high nitrate solution was prepared by adding 260 mL of ultra pure nitric acid (same acid as before) to 10 L of the high salt solution (prepared as before) to give an initial pH of 6.5 (I = 1.3953).

3.2 Design and Fabrication of Miniature Waste Packages

Miniature Waste Packages (MWP) were designed and fabricated to study the corrosion and transport processes under dynamic flow at two temperature regimes (25°C and 80°C). The MWP were constructed from low alloy steel (carbon steel). Table 4 shows the chemical analysis of carbon steel provided by the manufacturer. The use of carbon steel, rather than stainless steel, expedited the oxidation process and allowed us to carry out experiments within a reasonable time-frame (~28 days).

Table 4. Composition of Carbon Steel Used In MWP Fabrication[1]

Element (%)	Pipes and End Caps[2]	Basket and Rods[3]
Carbon	0.15	0.06
Manganese	0.73	0.25
Phosphorous	0.016	0.011
Sulfur	0.004	0.005
Silicon	0.014	0.007
Nickel	-	0.01
Aluminum	-	0.041
Copper	-	0.01
Iron	99.09	99.64
Cobalt	-	0.002
Vanadium	-	0.002

[1] Data from manufacturer. Non-Q, for corroborative use only.
[2] Searing Industries (Rancho Cucamonga, CA)
[3] California Steel Industries (Fontana,CA)

In our study, the MWP were also prepared to have interior features similar to the actual waste package containing DOE spent nuclear fuel (SNF) (Table 5). Each carbon steel MWP consisted of two pipes, an exterior pipe with end cap and a smaller internal pipe with five structural components added to simulate the "basket" inside the DOE SNF waste package, and rods placed in the internal pipe and basket areas to simulate glass pore canisters (GPC) and DOE canisters that would be present in the actual waste packages. In some of the MWP, in addition to explained internal features, iron shot were used to mimic design considerations to reduce void volume inside the actual waste packages. Figure 2 and Figure 3 exhibit side and end view of glass walled, iron shot packed MWP. Several such MWP were constructed with a glass exterior to allow study of internal oxidation patterns (see "Manner of Oxidation" below). When necessary, the MWP were sealed using Teflon tape and silicone sealant to prevent unwanted leaks and focus the flow-through the entrance and exit holes.

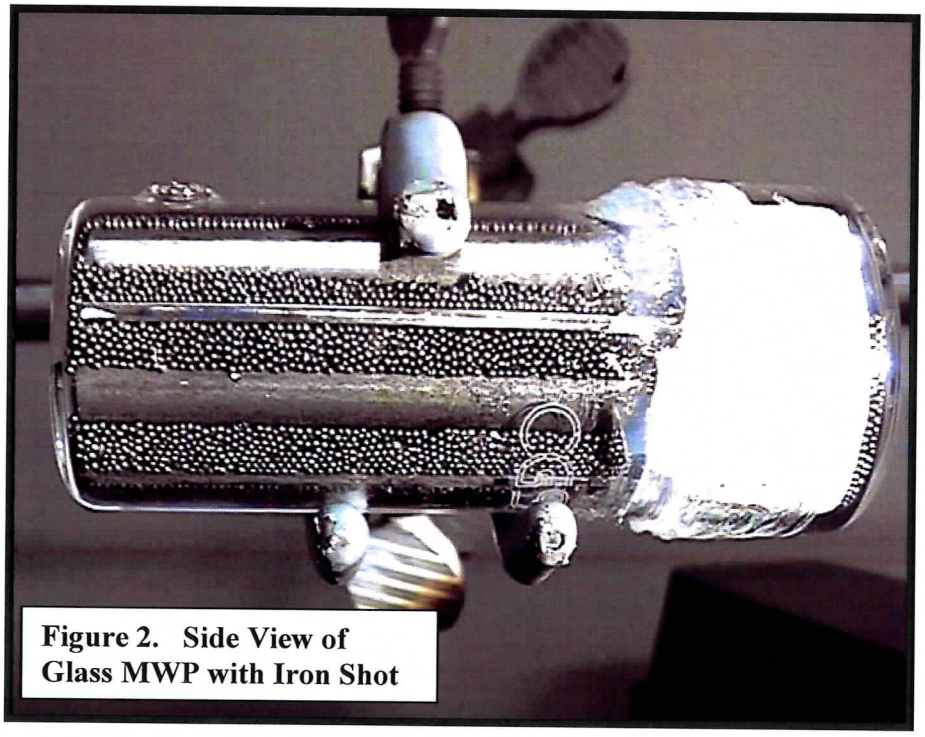

Figure 2. Side View of Glass MWP with Iron Shot

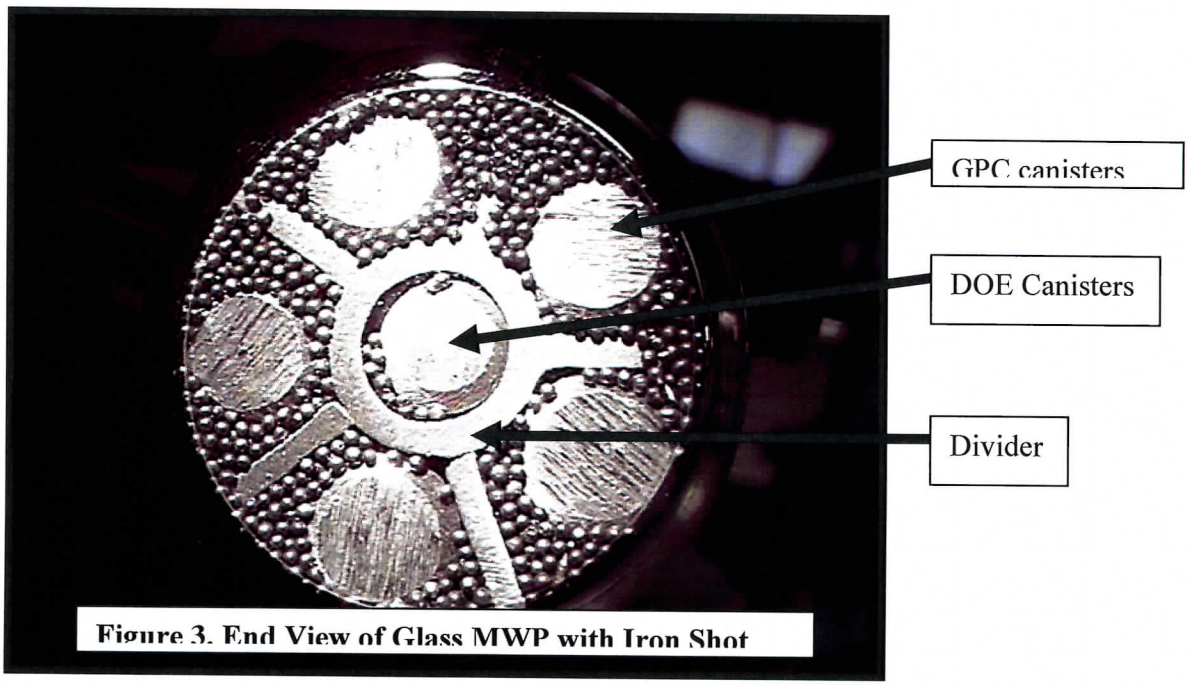

Figure 3. End View of Glass MWP with Iron Shot

Table 5. Dimensions and reduction factors for the actual waste package[1] versus the miniature waste package.

Component	Unit	Actual WP	MWP	Reduction Factor
I.D. of shell	cm	188.3	2.66	71
O.D. of basket core	cm	56.5	1.03	55
I.D. of basket core	cm	50.15	0.68	73
DOE Canister	cm	45.72	0.64	72
GPC Canister	cm	60.96	0.79	77
Inner shell surface area	cm^2	2.354×10^5	68.98	3400
Basket surface area[2]	cm^2	4.892×10^5	137.4	3560
DOE Canister surface area	cm^2	4.680×10^4	15.8	2960
GPC Canister surface area	cm^2	6.387×10^4	20.0	3200
Total surface area[2,3]	cm^2	1.138×10^6	339	3360
Total volume	cm^3	8.439×10^6	42.5	1.986×10^5

[1] Non-Q, for corroborative use only; [2] Includes dividers for MWP

Bathtub and flow-through models. "Bathtub" and "flow-through" configurations were employed to mimic different types of outflows from breached MWP (see Fig. 1). In the bathtub model, the test solution was introduced into the MWP from the top and exited from an opening in the end cap. In this scenario, most of the interior was flooded, i.e. saturated with water. In the flow-through model, test solution was again introduced from the top of the package, but exited instead from the bottom. In this configuration, the interior of the MWP was not necessarily entirely saturated with solution. For select experiments, a fine grain iron shot (1.5 mm average diameter with a density of 4.485 g/cm^3; Metaltec Steel Co., Canton, MI) was added to fill the void space within the MWP. The quantity of iron shot present in each MWP was determined by weight. Figures 4 and 5 show the side and end views of a glass MWP filled with iron shot. The glass MWP were used primarily to observe the "manner of oxidation" occurring within the MWP during the experiments.

3.3 Introduction of Test Solutions to the Miniature Waste Packages

We introduced the test solutions to the MWP using a peristaltic pump (Carter 12/8 Cassette Pump, Model 740128; Manostat; Barrington, IL) (Fig. 4). The average flow rate was 29.9 ± 5.1 (1 S.D.) (range: 18.8 to 37.9 mL/day), which is similar to the estimated

rate of water movement at Yucca Mountain (CRWMS M&O 2000b). The solutions were delivered with flexible tubing "cassette links" of either 0.25 or 0.89 mm inside diameter. The cassette links were coupled with Teflon tubing of similar diameter on both ends to span the distance between the pump and the solutions on one side and between the pump and the MWP on the other side. The pump is equipped with 12 cassettes allowing 12 separate flows to be used for the experiment. To prevent the tubing from floating to the surface of the test solution reservoir, we passed the transfer tubing through a hole bored in the bottom of a 100 mL polypropylene graduated cylinder and set the graduated cylinder into the solution reservoir.

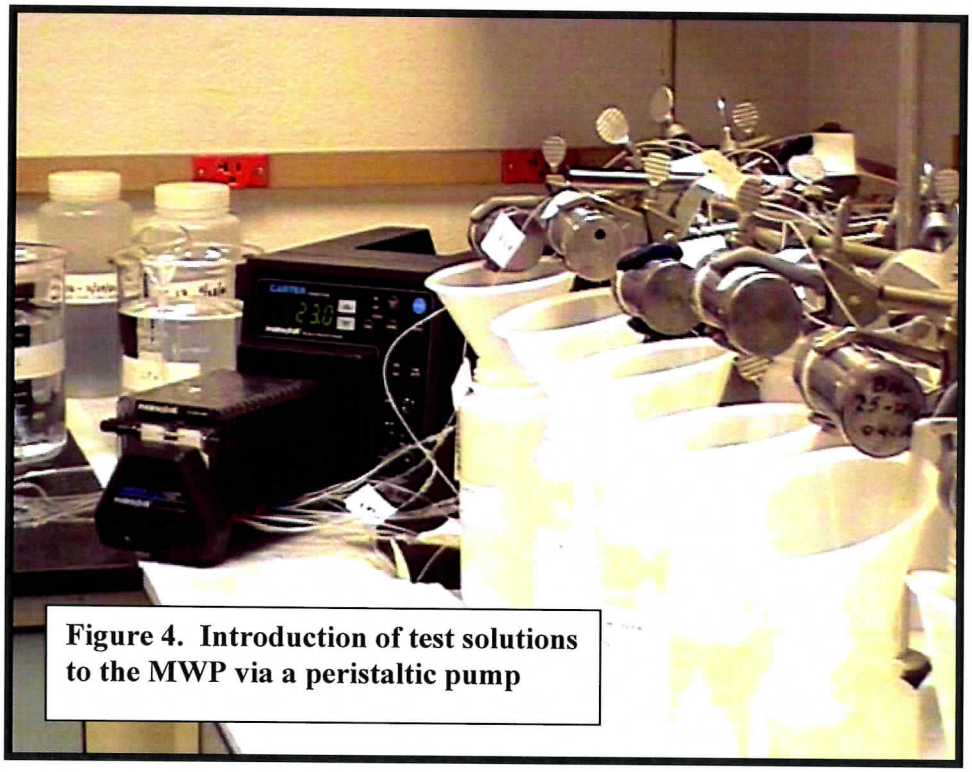

Figure 4. Introduction of test solutions to the MWP via a peristaltic pump

The pump was calibrated in accordance with UNLV-IPLV-053 (Determination of Flow Rate Using the Carter Cassette Pump). Briefly, for calibration the pump was operated over a timed interval of at least 4 hours transferring solution to a weighed beaker. The flow rate (mL/day) was determined by dividing the mass of solution transferred (grams) by the time (days), and dividing the result by the density of the solution (g/mL).

3.4 Monitoring of pH, Conductivity and Dissolved Oxygen

Influent (time 0) and effluent from the MWP were monitored during the experiment for changes in pH, conductivity, and dissolved oxygen (DO) on at least a weekly basis. The measurements were taken using standard procedures and in accordance with IPLV-012 (Measurement of Total Dissolved Solids, Conductivity, Alkalinity, and pH in Water Samples) and IPLV-056 (Measurement of Dissolved Oxygen in Water Samples). The pH and conductivity (μSm) was determined with a standard meter (Corning Model 442;

Corning, NY). Dissolved oxygen was determined with a standard DO meter (VWR; Plainsfield, NJ) and reported in ppm.

3.5 Segregation and Quantification of Suspended Solids in the Effluent

Sequential Filtration. To segregate and quantify suspended solids in the MWP effluent, the effluent was collected on a weekly basis into 250 mL polypropylene containers and filtered sequentially through previously weighed (to the nearest 0.0001g) Teflon filters (Durapore; Millipore Corporation) with pore sizes of 0.45 μm, 0.22 μm, and 0.10 μm, respectively. Next, the filters were allowed to air dry, reweighed, and amount of filtered solids (in grams) was determined by difference. The filtrate (the solution remaining after passing through the 0.10 μm filter) was saved for determination of "dissolved" iron (see Dissolved Iron below).

The filters from the high saline and high saline – high nitrate solutions required "washing" to remove (dissolved) salt that tended to recrystallize on the filters. This was needed to obtain an accurate measure of the quantity of corrosion products in the MWP effluent. In the initial tests (EXP I) with these solutions, the filters were first dried and subsequently washed with approximately 500 mL of de-ionized water (>18.3MΩ; Nanopure, Dubuque, IA). The filters were then allowed to dry again and a final weight was taken. In subsequent tests (EXP II), after completing the filtering and saving the filtrate, the filters were additionally washed with approximately 250 mL of de-ionized water (prior to drying). They were then dried and the final weight taken.

Dissolved Iron. MWP influent (i.e., test solutions) and effluent were analyzed by sector field inductively coupled plasma mass spectrometry (ICP-MS; VG Axiom, Wilshire, UK) to determine the concentration of dissolved iron. This device produced signals of ~ 10^6 counts/sec for 1 μg/L ^{54}Fe and a m/z 220.5 background of < 0.5 counts/sec using a self-aspirating PFA capillary nebulizer (CPI International, Santa Rosa, CA). The Axiom's sample introduction system consisted of a cyclonic spray chamber followed in series by a water-cooled bead impact spray chamber.

Briefly, select samples were diluted approximately 1:300 with 1% nitric acid (SeaStar, Seattle WA) gravimetrically (by analytical balance). The dilutions were necessary to decrease the quantity of total dissolved solids (particularly for the salt solutions) to prevent instrumental drift due to buildup of material on the cones of the ICP-MS interface, and to decrease the concentration of the iron in solution so that it was in the working (calibration) range. Prior to analyses, the solutions were spiked to ~1 ppb with ^{89}Y which acted as the internal standard. Instrumental parameters, gas flows and torch position, were optimized daily. Data were collected in the scan mode at m/z 54 using a dwell time of 0.4 ms, 40 points per mass spectral peak, over a m/z interval of 3 peak widths. Three acquisitions were collected for each sample solution. The instrument was calibrated using commercially available (NIST traceable) mixed element standards solutions (Ultra-Scientific and Perkin Elmer Corporation; Norwalk, CT). For quality control, each set of samples was accompanied by a blank and a standard reference

material (NIST 1640 or 1643d). A resolving power of approximately 3000 (medium resolution) was used to resolve isobaric interferences for iron.

3.6 Characterization of Transported Material

X-Ray Diffraction Analyses. Selected filters were forwarded to the Nevada Bureau of Mines and Geology at the University of Nevada Reno for X-ray Diffraction (XRD) analysis (Philips 3100 Automated Diffractometer) to identify mineral components (IPLV-046; Operation of X-Ray Diffractometer).

Particle Size Distribution. Particle sizes of the filtered solids were estimated by inspecting select filters with a scanning electron microscope (Joel JSM-5600, Jeol Inc., Peabody, MA) at the University of Nevada Las Vegas Geology Department. An EDS spectra was used to help identify the particles (e.g., iron oxides or salt crystals).

3.7 Manner of Oxidation

A digital video camera (JVC Inc., Model GR-DV2000) was used to document corrosion patterns of the MWP throughout the experiment for both the glass and carbon-steel MWP.

3.8 Experimental Phases Discussed in the Report

Experiments were conducted in three distinct phases: Scoping, Experiment I, and Experiment II. In the Scoping phase, we developed the MWP and did some initial testing of procedures and equipment. During this phase, we used several MWP with glass exteriors to study the manner of oxidation through time-lapse photography within the confines of the MWP. The second phase (Experiment I) conducted during the summer of 2002 focused on introducing the four test solutions into the carbon-steel MWP and subsequent effluent collection and analyses. The third phase (Experiment II) was conducted during the Winter of 2002-2003 and essentially replicated the first experiment (utilizing some of the experience we gained in experiment I) except that we did not include J-13 due to limited supply and pump-related issues.

3.9 Control of electronic data

Data, such as conductivity and pH, were manually entered into electronic spreadsheets for processing. The data was transferred directly from the notebook usually on the same day it was collected. Each data was visually inspected upon entering the values and later spot-checked to verify that there were no mistakes made in the transfer. Data was stored on the HRC network server, which is backed up nightly. In addition, data was protected through use of passwords and secured offices and laboratories.

4. Results and Discussion

4.1 Manner of Oxidation

The oxidation patterns within the MWP varied by model configuration (i.e., bathtub versus flow-through) and solution chemistry (e.g., pH and salinity). A digital camera recorded the external corrosion patterns of the MWP at various stages of the experiment. Selected images, highlighting attributes of the corrosion process, are presented in this section. The images proved useful in studying the "manner of oxidation" of the MWP. Figures 6, 7 and 8 present a typical MWP and the setup for flow-through and bathtub MWP experiments. The experiments were conducted at 25 and 80 °C. Figure 9 presents the setup for the 80 °C experiment. However, no liquid exited from MWP at this temperature, even at 100% humidity levels. Consequently, there were no more experiments conducted and no data will be reported for this temperature.

Low pH experiments of the bathtub and flow-through resulted in formation of corrosion products that appeared to consist of smaller size suspended particles (Figures 10 and 11). Upon clogging of exit holes especially in the bathtub models the overflow caused severe corrosion on the exterior surface of the MWP, especially at the bottom where overflow water collected before dripping (Fig. 12)

In the high salt experiments (both with and without iron shot), the bathtub models accumulated oxidation products at the exit hole and in most cases completely clogged the exit hole by the end of the fourth week (Figs. 13 and 14). This self-sealing is likely due to the larger molar volume of the corrosion products. Gu et al (1999) studied zero valence iron as permeable reactive barriers and concluded that precipitation of iron oxyhydroxides could count for void volume reduction of 10-15% of iron packed columns and could reduce porosity to 0.42 from the original porosity of 0.5. The flow-through model experiments resulted in formation of salt crystals at and near the bottom exit hole. Recrystalization of salt on the exterior of MWP could cause accelerated corrosion at the later times (Fig. 15). This is important because excessive corrosion, especially in the bottom, will promote corrosion and, over time, increase the likelihood of bottom failure.

Glass walled MWP were used to evaluate internal corrosion patterns. Figures 16 and 17 shows the result of J-13 inflow over a span of 32 days. Formation of reddish brown, green and black corrosion products of iron is evident. The interior of the MWP appears to corrode at a higher rate compared to the portion of the rods touching the glass walls. Poor circulation of water where the rods contacted the glass may have produced conditions that resulted in formation of a black corrosion product. We believe this to be magnetite because when a magnet was placed against the glass wall, the black corrosion products were attracted to it. Magnetite (Fe_3O_4) is known to be a black paramagnetic mineral. Through time-lapse digital photography, we were able to document corrosion patterns including formation of a thin-layer of corrosion products on the rods and dividers within MWP. In addition, we observed the entrainment of smaller corrosion products out of MWP and settling of larger corrosion particles on the bottom of the MWP.

MWP, where the exit hole clogged resulted in overflow of solution at the entrance site, spillage around the MWP, and eventually drip from the bottom. Thus, a skirt composed of stainless steel or other corrosion resistant material, positioned around the bottom of the actual waste package to deflect dripping water away from the bottom of the waste package may prevent or delay corrosion of the waste package, particularly at the bottom which is more susceptible to degradation (Fig 5).

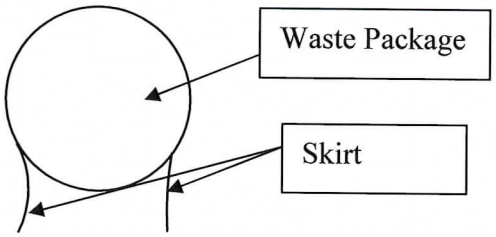

Figure 5. Addition of Skirt to the Sides of Waste package

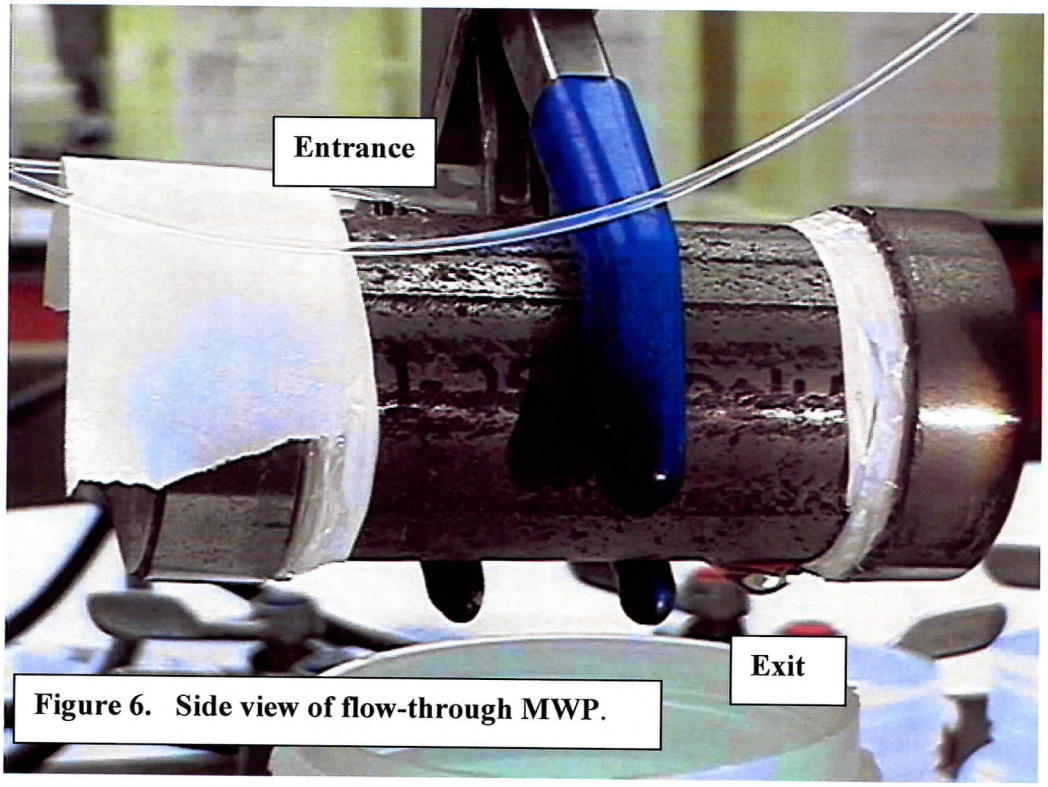

Figure 6. Side view of flow-through MWP.

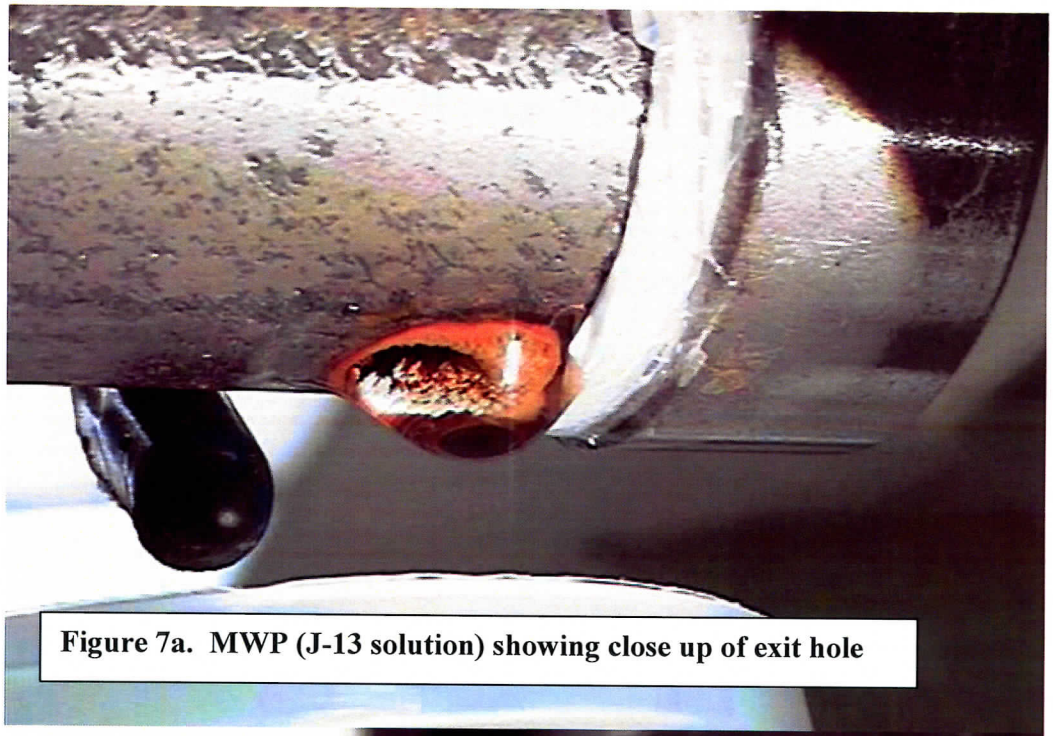

Figure 7a. MWP (J-13 solution) showing close up of exit hole

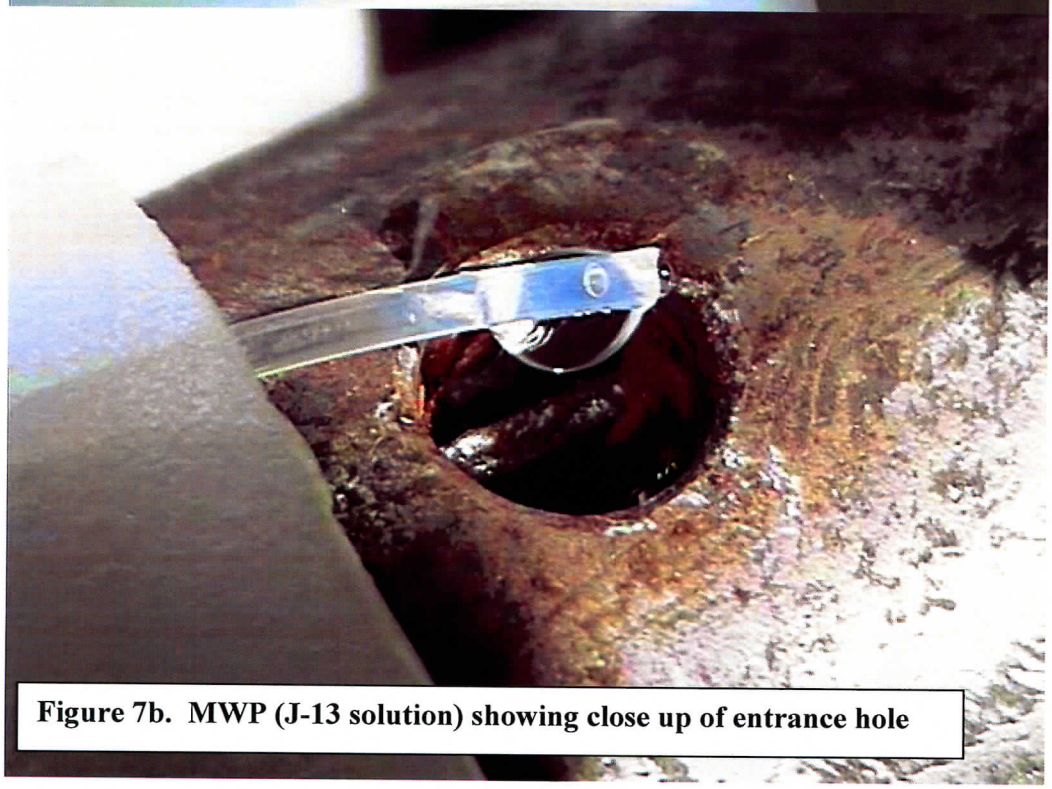

Figure 7b. MWP (J-13 solution) showing close up of entrance hole

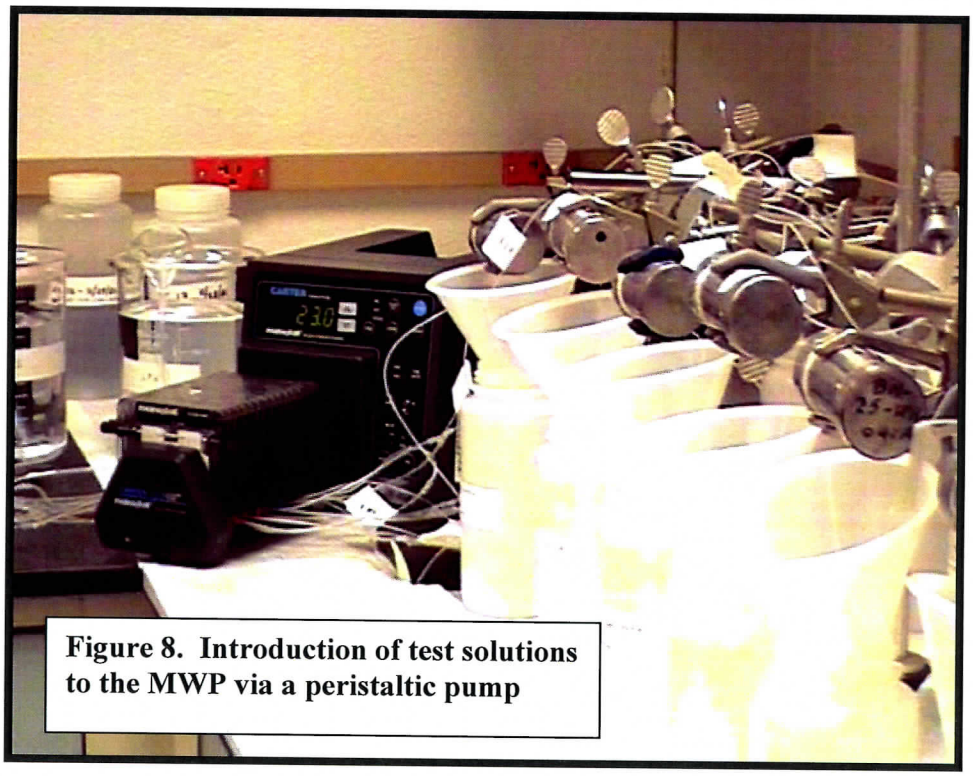

Figure 8. Introduction of test solutions to the MWP via a peristaltic pump

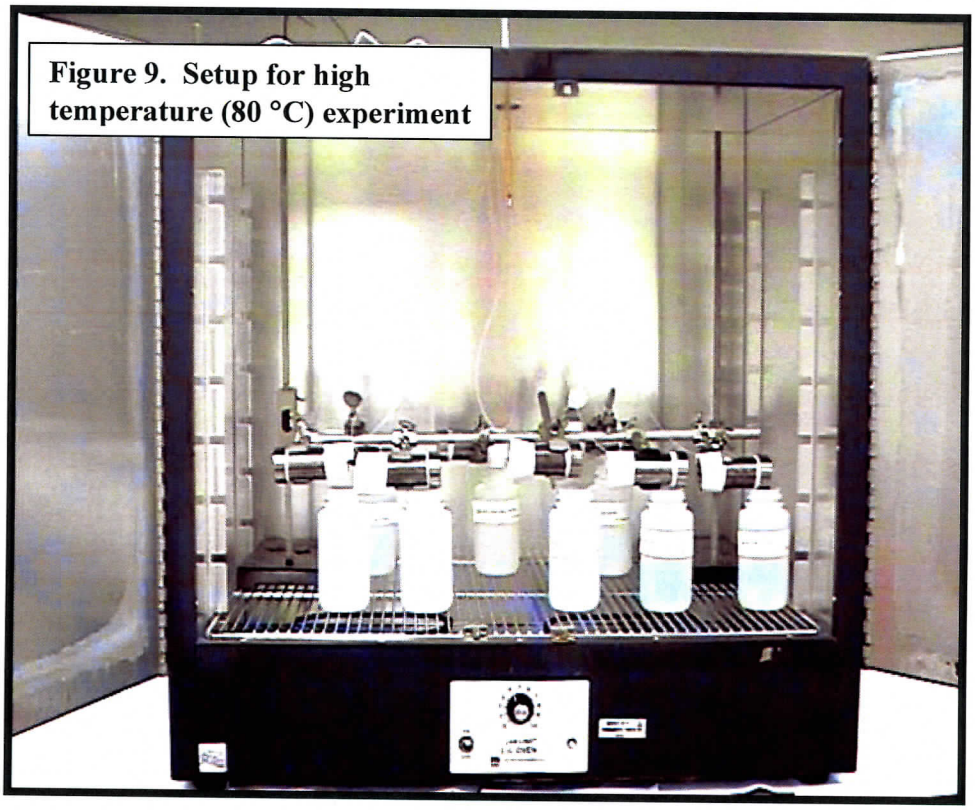

Figure 9. Setup for high temperature (80 °C) experiment

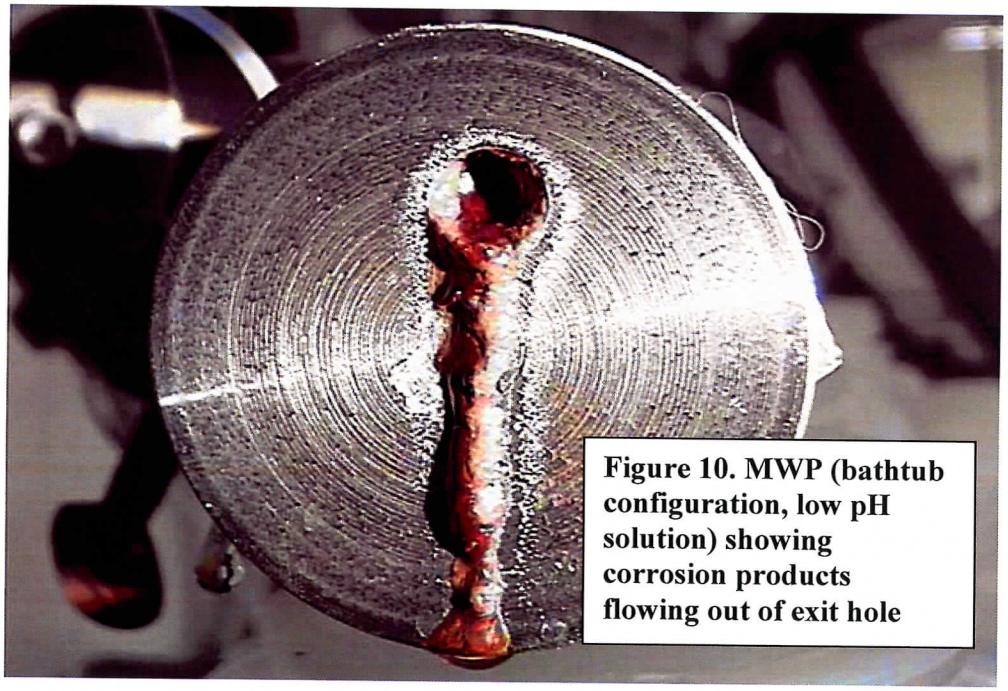

Figure 10. MWP (bathtub configuration, low pH solution) showing corrosion products flowing out of exit hole

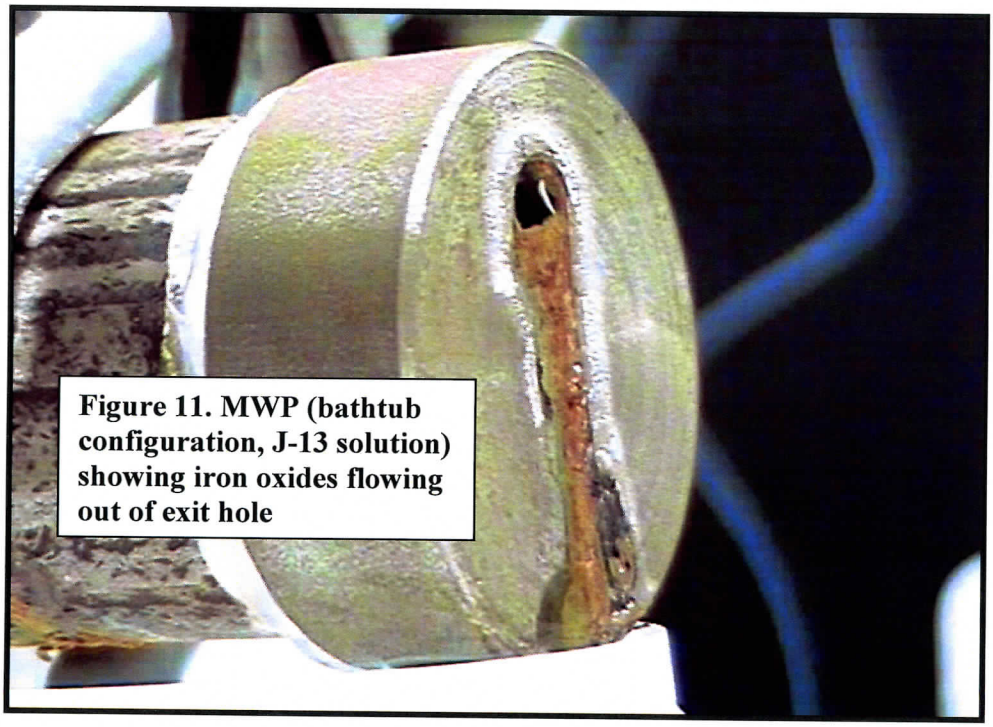

Figure 11. MWP (bathtub configuration, J-13 solution) showing iron oxides flowing out of exit hole

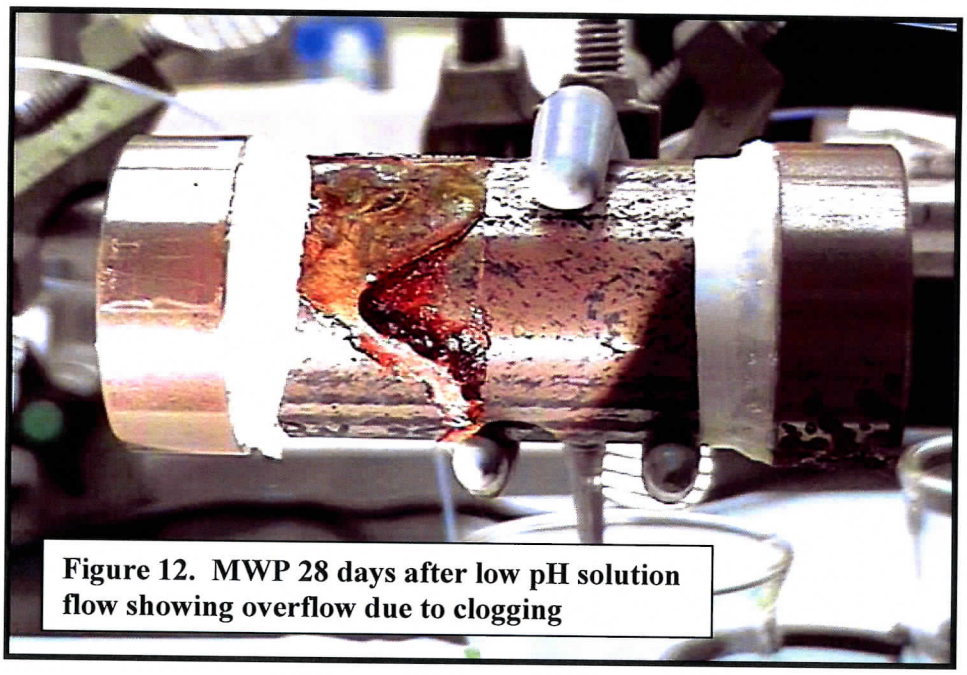

Figure 12. MWP 28 days after low pH solution flow showing overflow due to clogging

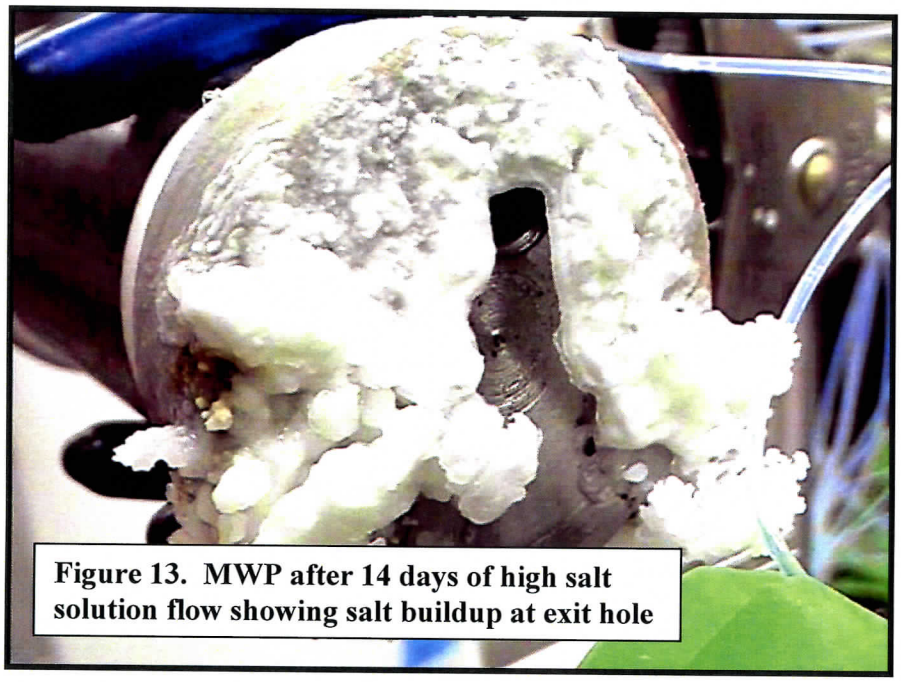

Figure 13. MWP after 14 days of high salt solution flow showing salt buildup at exit hole

Figure 14. MWP after 14 days of high salt-high nitrate solution flow showing salt buildup and iron oxides at exit hole

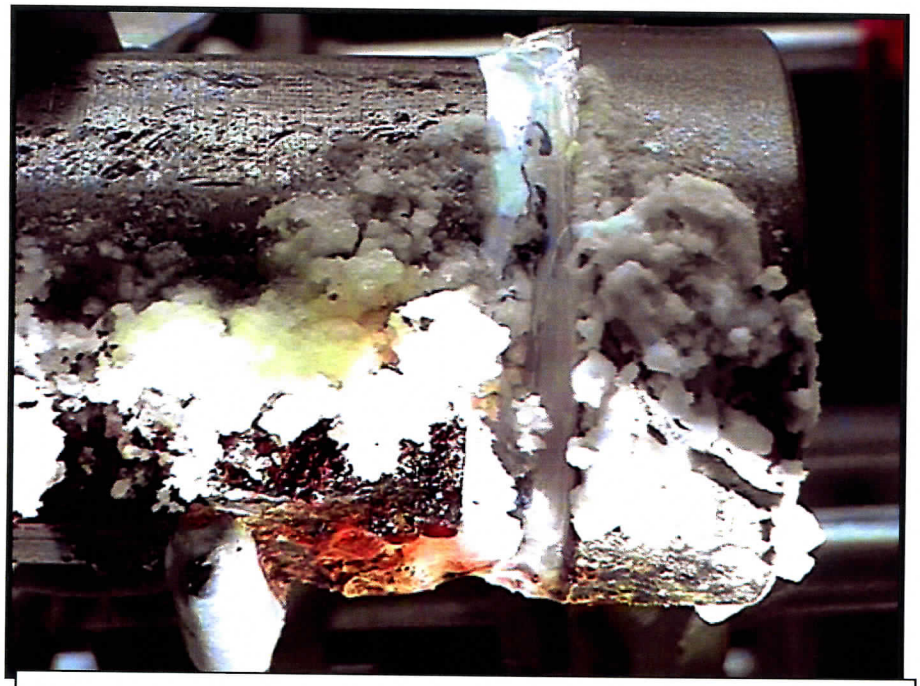

Figure 15. MWP after 14 days of high salt – high nitrate solution showing corrosion pattern on bottom of package

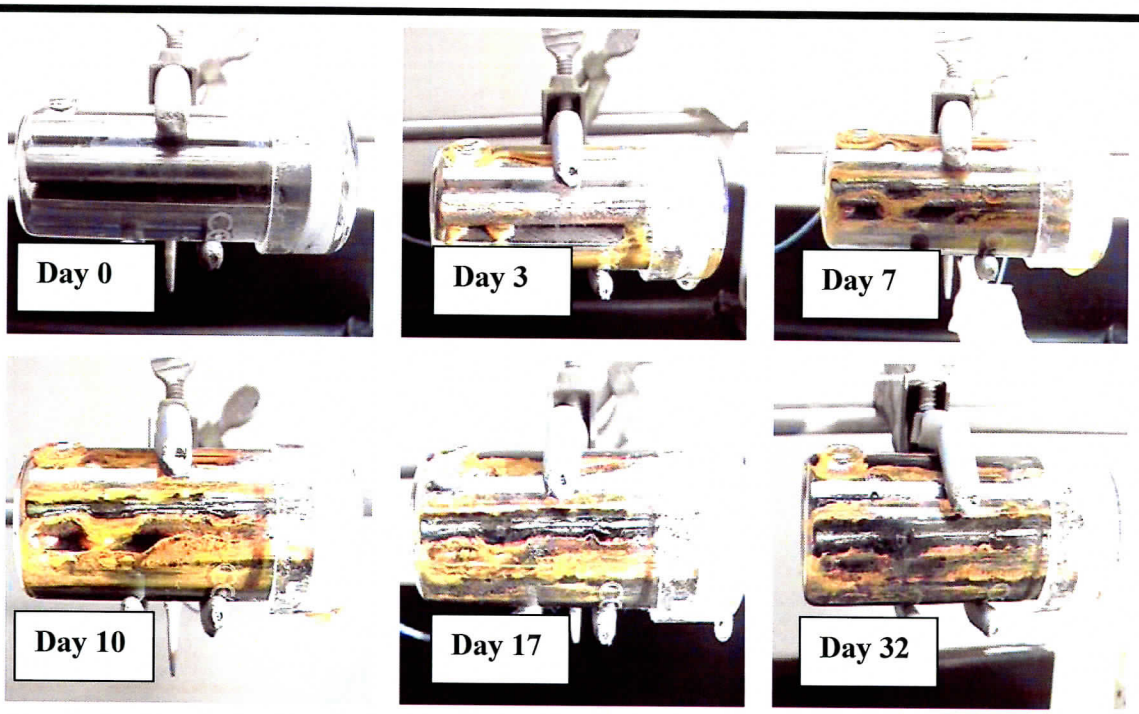

Figure 16. Time-Lapse Photos Showing Corrosion Process in Glass MWP Without Iron Shot using J-13 water (side view)

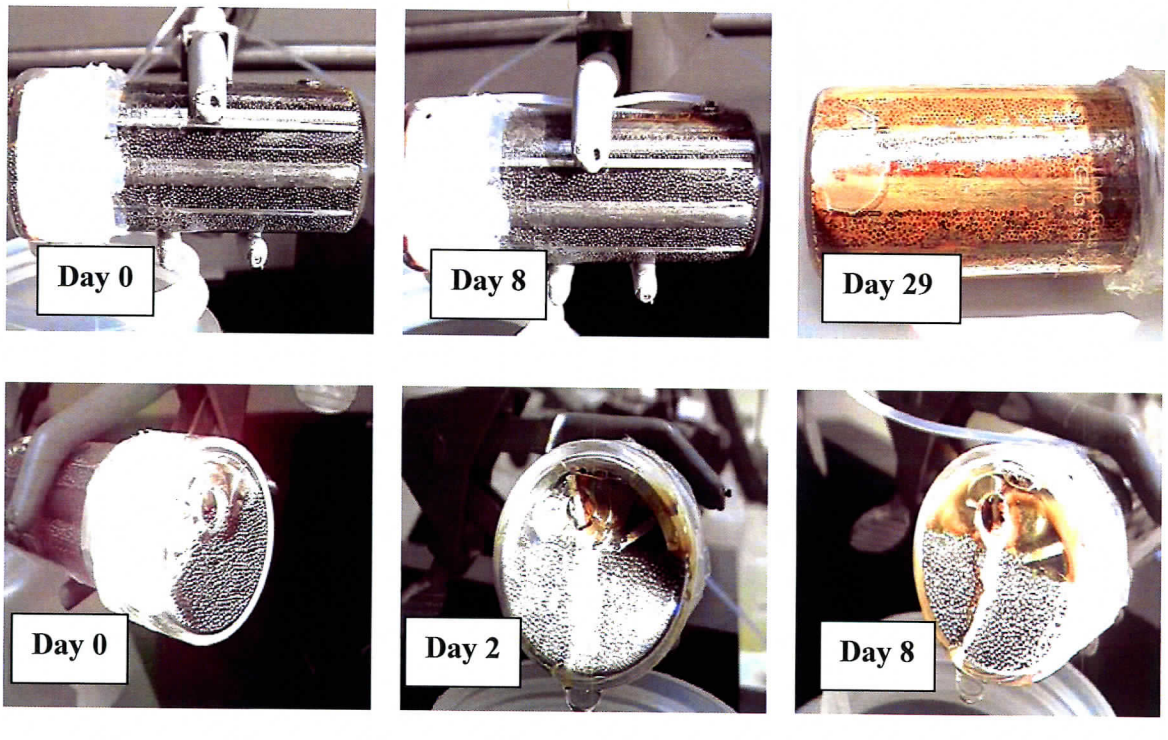

Figure 17. Time-Lapse Photos Showing Corrosion Process in Glass MWP for J-13 solution (with iron shot)

4.2 Quantification of Transported Materials

To quantify the transport of soilds (corroded iron) from MWP, no differentiation was made between solids with average diameters smaller than 0.1 μm and "dissolved" components in the effluent. Tables 6 (EXP I) and 8 (EXP II) are summaries of average concentration of solids in different effluents of MWP by particle size. In experiments where J-13 well water was used as inflow, on average 99% by mass of the transported solids in the MWP effluent were particles with average diameters greater than 0.1μm. The remaining 1% of corrosion products in the effleuent were "dissolved" products (Figure 18). In the case of high nitrate-high salt inflow, more than 97% of transported solids exiting the MWP were particles with average sizes greater than 0.1μm (Fig 20). In contrast, the low pH solution had only 11.5% of the solid particles in the outflow with average sizes greater than 0.1μm and 88.5% were smaller than 0.1μm or dissolved (Figure 20). There is a great contrast in mass/filter size distribution between the low pH and the other two types of inflow solutions (control and high salts). The excess concentration of H^+ in low pH solution could retard formation of $FeOH^+$ which contributes to formation of $Fe(OH)_2$ and green rust complexes.

Tables 6 and 8 also shows the average mass of solids in the outflow of the MWP under different types of inflow. Total average for all inflow conditions is 20.7 mg/L(EXP I) and 44.8 mg/L (EXP II) . In the control samples the average mass from MWP with iron shot was higher, possibly due to larger internal surface area. The average mass flow of control samples was 16.5 mg/L. The two high salt inflows produced average mass flows of about 20.2 mg/L (EXP I) and 37.8 mg/L (EXP II). The amount of solids were produced from low pH inflow averaging about 26.0 mg/L (EXP I) and 27.2 (EXP II).

Table 6: Average Concentration of Solids in the Effluent (EXPI)

MWP NUMBER	AVERAGE FLOW RATE mL / Day	SOLIDS ON .45 µm (mg)	SOLIDS ON .22 µm (mg)	SOLIDS ON .1 µm (mg)	TOTAL SOLIDS (mg)	No. of Days (Days)	Mass Flow of Filtered Solids[1] (mg/L)
BN-25-C-001A	26.73	9.1000	1.7000	0.6000	11.4000	28	15.2313
BN-25-C-001B	25.60	12.6000	2.0000	0.8000	15.4000	28	21.4819
BI-25-C-002A	32.55	5.0000	1.7000	0.5000	7.2000	28	7.9004
BI-25-C-002B	31.82	6.2000	1.4000	0.8000	8.4000	28	9.4294
FN-25-C-003A	33.80	22.9000	1.4000	0.7000	25.0000	28	26.4156
FN-25-C-003B	30.64	19.9000	1.7000	1.0000	22.6000	28	26.3394
FI-25-C-004A	32.81	10.1000	1.3000	0.8000	12.2000	28	13.2819
FI-25-C-004B	26.67	6.4000	1.5000	1.2000	9.1000	28	12.1853
Average							16.5+/- 7.7
BN-25-HS-005A	36.62	8.1000	1.3000	1.0000	10.4000	24	11.8321
BN-25-HS-005B	25.24	8.6000	2.8000	2.6000	14.0000	24	23.1076
BI-25-HS-006A	30.05	6.0000	1.6000	3.3000	10.9000	24	15.1127
BI-25-HS-006B	31.56	7.5000	1.9000	4.2000	13.6000	24	17.9557
FN-25-HS-007A	30.11	6.9000	17.9000	7.2000	32.0000	24	44.2794
FN-25-HS-007B	26.65	7.8000	2.4000	2.9000	13.1000	24	20.4800
FI-25-HS-008A	37.80	5.1000	2.1000	5.6000	12.8000	24	14.1091
FI-25-HS-008B	37.91	3.9000	1.7000	1.9000	7.5000	24	8.2431
Average							19.4+/-9.1
BN-25-LPH-009A	34.07	19.3000	10.0000	11.5000	40.8000	24	49.8900
BN-25-LPH-009B	33.82	8.0000	3.0000	3.3000	14.3000	24	17.6155
BI-25-LPH-010A	34.24	9.0000	5.2000	4.0000	18.2000	24	22.1475
BI-25-LPH-010B	34.65	10.8000	9.1000	9.5000	29.4000	24	35.3536
FN-25-LPH-011A	37.30	9.8000	3.0000	1.9000	14.7000	24	16.4222
FN-25-LPH-011B	37.87	15.2000	1.5000	5.7000	22.4000	24	24.6435
FI-25-LPH-012A	27.87	9.5000	0.9000	1.8000	12.2000	24	18.2377
FI-25-LPH-012B	32.91	15.0000	1.6000	1.8000	18.4000	24	23.2926
Average							26.0+/-6.5
BN-25-HS-HN-013A	34.52	9.4000	3.7000	3.9000	17.0000	24	20.5185
BN-25-HS-HN-013B	31.09	11.3000	1.4000	2.4000	15.1000	24	20.2355
BI-25-HS-HN-014A	26.93	10.4000	1.3000	2.2000	13.9000	24	21.5054
BI-25-HS-HN-014B	34.27	9.8000	0.8000	1.5000	12.1000	24	14.7095
FN-25-HS-HN-015A	33.78	19.3000	2.0000	1.6000	22.9000	24	28.2485
FN-25-HS-HN-015B	29.16	15.8000	1.0000	2.6000	19.4000	24	27.7221
FI-25-HS-HN-016A	36.94	16.2000	1.4000	2.0000	19.6000	24	22.1107
FI-25-HS-HN-016B	32.70	6.5000	1.6000	1.8000	9.9000	24	12.6146
Average							21.0+/-4.9
Total Average							20.7+/- 3.4

NOTES: Explanation of abbreviations is listed in the "Key for Select Abbreviation" Section

1. Mass Flow (mg/L) = Total Solids/((Ave. Flow Rate)(No. of Days)(1000 mL/L)); Data Source: DID# 034JC.002

Table 7 is a summary of iron inventory by converting mass of solids corrosion products to iron. Goethite (FeOOH) was considered as a typical corrosion product and the amount of solids collected on different filter sizes was assumed to goethite, which was converted to equivalent mass of iron (molar ratio of Fe^0 to FeOOH is 1:1). Figures 18 and 19 shows percent distribution and inventory (mass distribution) of iron as a function of particle size in the effluent.

Table 7. Total Iron Inventory in the MWP outflow (mg) for Experiment I [1,2,3]

MWP	Iron Mass on 0.45 μm Filters	Iron Mass on 0.22μm Filters	Iron Mass on 0.10 μm Filters	Mass of Dissolved Iron[3]	Total
BN-25-C-001A	5.7	1.1	0.4	0.2	7.3
BI-25-C-002A	3.1	0.9	0.3	0.05	4.4
FN-25-C-003A	14.4	1.1	0.4	0.1	16.0
FI-25-C-004A	6.4	0.8	0.5	0.03	7.7
BN-25-HS-005A	5.1	0.8	0.6	7.2	13.8
BI-25-HS-006A	3.8	1.0	2.1	14.5	21.3
FN-25-HS-007A	4.3	11.3	4.5	15.5	35.7
FI-25-HS-008A	3.2	1.3	3.5	14.6	22.7
BN-25-LPH-009A	12.2	6.3	7.2	91.1	116.8
BI-25-LPH-010A	5.7	3.3	2.5	90.2	101.6
FN-25-LPH-011A	6.2	1.9	1.2	115	124.2
FI-25-LPH-012A	6.0	0.6	1.1	25.8	33.4
BN-25-HS-HN-013A	5.9	2.3	2.5	1.8	12.6
BI-25-HS-HN-014A	6.5	0.8	1.4	0.9	9.7
FN-25-HS-HN-015A	12.2	1.3	1.0	1.3	15.7
FI-25-HS-HN-016A	10.2	0.9	1.3	1.3	13.7

NOTES: Explanation of abbreviations is listed in the "Key for Select Abbreviation" Section

1.Duration of the experiments was 24 days and the average volume of effluent was 569 mL.

2.Assuming goethite (FeO(OH)) as the most commonly identified corrosion product and converting it to equivalent iron.

3.Data calculated as follows: the average iron concentration in μg/g (ppm) obtained from ICP-MS analysis (UCCSN Data ID #034JC.006) was multiplied by the weight of solution (g) (UCCSN Data ID #034JC.007) and by a factor of 1000 to give mass (mg). For example, for BN-25-LPH-009A the average concentration found by ICP-MS was 111.7 μg/g. Multiplying this value by the weight of solution (816 g) and dividing by 1000 gives the mass of 91.1 mg.

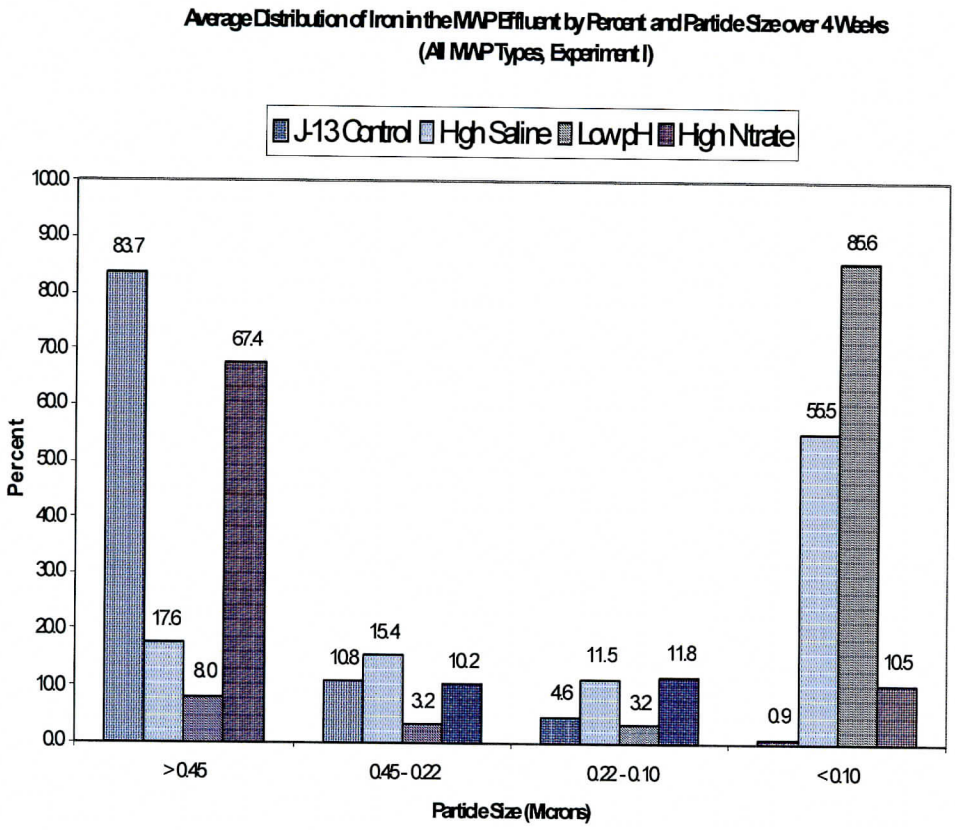

Fig. 18. Average Distribution of Iron in the MWP Effluent by Percent and Particle Size Over 4 Weeks (All MWP Types, EXP I). The graph was generated from UCCSN Data #034JC.002 and #034JC.007 as follows: total mass of solids from the A runs (from worksheet "solids by filter size") were multiplied by the percent mass of iron (0.629) in geothite (FeO(OH)) and by 1000 to change the units to mg of iron.

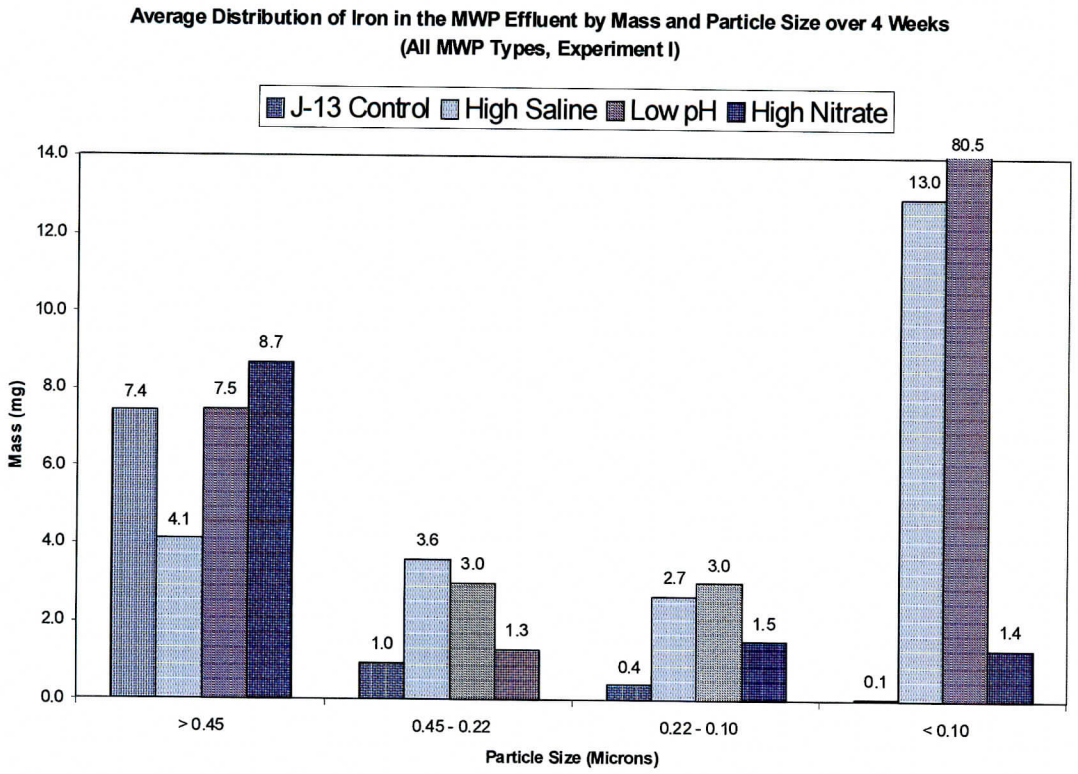

Fig. 19. Average Distribution of Iron in the MWP Effluent by Mass and Particle size over 4 weeks (All MWP Types, EXP I). See legend in Fig. 18 for calculation details.

Tables 8 and 9 contain data on the average mass of solids and iron inventory performed in experiment II (EXP II). Experiment II was conducted to assure that procedures used for washing filters in high salinity and low pH experiments were sufficient to produce accurate data. Data in these tables show higher amount of solids on the filters for high salt solutions (regardless of the presence of nitrate) but very little difference on low pH results between the two experiments. Figures 20 and 21 show the average concentration of solids and inventory of iron in the effluents of different experiments repeated for EXP II.

Table 8 : Average Concentration of Solids in the Effluent (EXPII)[1]

MWP NUMBER	AVERAGE FLOW RATE (mL/Day)	SOLIDS 0N 0.45 µm (mg)	SOLIDS 0N 0.22 µm (mg)	SOLIDS 0N 0.10 µm (mg))	TOTAL SOLIDS (mg)	No. of Days (Days)	Mass Flow of Filtered Solids[1] (mg/L)
BN-25-HS-037A	27.47	13.6000	5.4000	6.5000	25.5000	28	33.1480
BN-25-HS-037B	22.36	7.6000	6.9000	5.3000	19.8000	28	31.6252
FN-25-HS-039A	23.8	12.4000	3.8000	7.3000	23.5000	28	35.2590
FN-25-HS-039B	24.93	9.5000	4.0000	2.7000	16.2000	28	23.2124
Average							30.8125
BN-25-LPH-041A	23.79	9.1000	3.4000	3.1000	15.6000	28	23.4157
BN-25-LPH-041B	25.82	13.0000	5.4000	10.6000	29.0000	28	40.1093
FN-25-LPH-043A	21.76	9.3000	3.5000	1.7000	14.5000	28	23.8007
FN-25-LPH-043B	18.76	7.7000	2.8000	0.8000	11.3000	28	21.5114
Average							27.2075
BN-25-HS-HN-045A	23.44	16.5000	6.3000	4.0000	26.8000	28	40.8371
BN-25-HS-HN-045B	28.12	12.2000	3.1000	4.2000	19.5000	28	24.7705
FN-25-HS-HN-047A	25.04	31.5000	8.0000	5.0000	44.5000	28	63.4810
FN-25-HS-HN-047B	20.62	22.8000	3.6000	2.6000	29.0000	28	50.2384
Average							44.8325

NOTES: Explanation of abbreviations is listed in the "Key for Select Abbreviation" Section

[1] Mass Flow (mg/L) = Total Solids/((Ave. Flow Rate)* (No. of Days)(1000 mL/L)); Data Source: DID#, 034JC.004.

Table 9. Total Iron Inventory in the MWP outflow (mg) for Experiment II [1,2,3]

MWP	Iron Mass on 0.45 μm Filters	Iron Mass on 0.22μm Filters	Iron Mass on 0.10 μm Filters	Mass of Dissolved Iron[3]	Total
BN-25-HS-037A	8.6	3.4	4.1	7.8	23.9
BN-25-HS-037B	4.8	4.3	3.3	6.2	18.6
FN-25-HS-039A	7.8	2.4	4.6	3.6	18.4
FN-25-HS-039B	6.0	2.5	1.7	3.9	14.1
BN-25-LPH-041A	5.7	2.1	2.0	86.7	96.5
BN-25-LPH-041B	8.2	3.4	6.7	89.1	107.4
FN-25-LPH-043A	5.9	2.2	1.1	82.0	91.1
FN-25-LPH-043B	4.8	1.8	0.5	82.0	89.1
BN-25-HS-HN-045A	10.4	4.0	2.5	0.5	17.4
BN-25-HS-HN-045B	7.7	2.0	2.6	0.6	12.9
FN-25-HS-HN-047A	19.8	5.0	3.1	0.5	28.5
FN-25-HS-HN-047B	14.4	2.3	1.6	0.4	18.7

NOTES: Explanation of abbreviations is listed in the "Key for Select Abbreviation" Section

1.Duration of the experiments was 28 days and the average volume of effluent was 569 mL.

2. Assuming goethite (FeO(OH)) as the most commonly identified corrosion product and converting it to equivalent iron.. In the case of dissolved iron mass was converted to equivalent moles of goethite.

3.Data from ICP-MS Analysis (see note in Table 7 for calculation details).

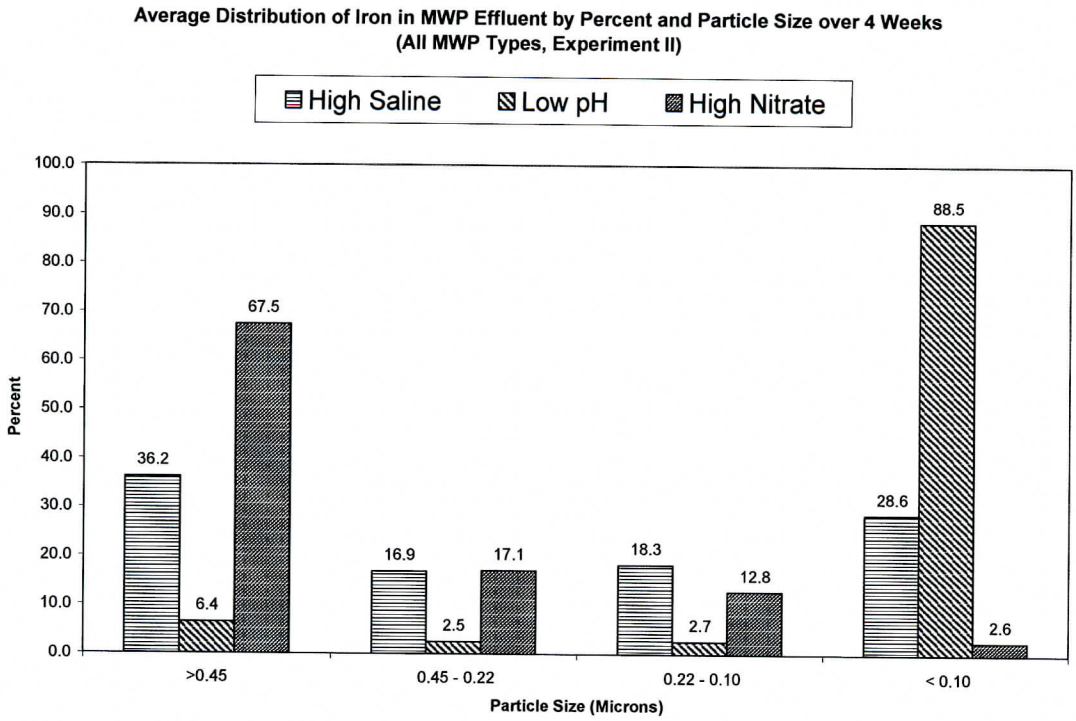

Fig. 20. Average Distribution of Iron in the MWP Effluent by Percent and Particle Size Over 4 Weeks (All MWP Types, EXPII). See legend in Fig. 18 for calculation details.

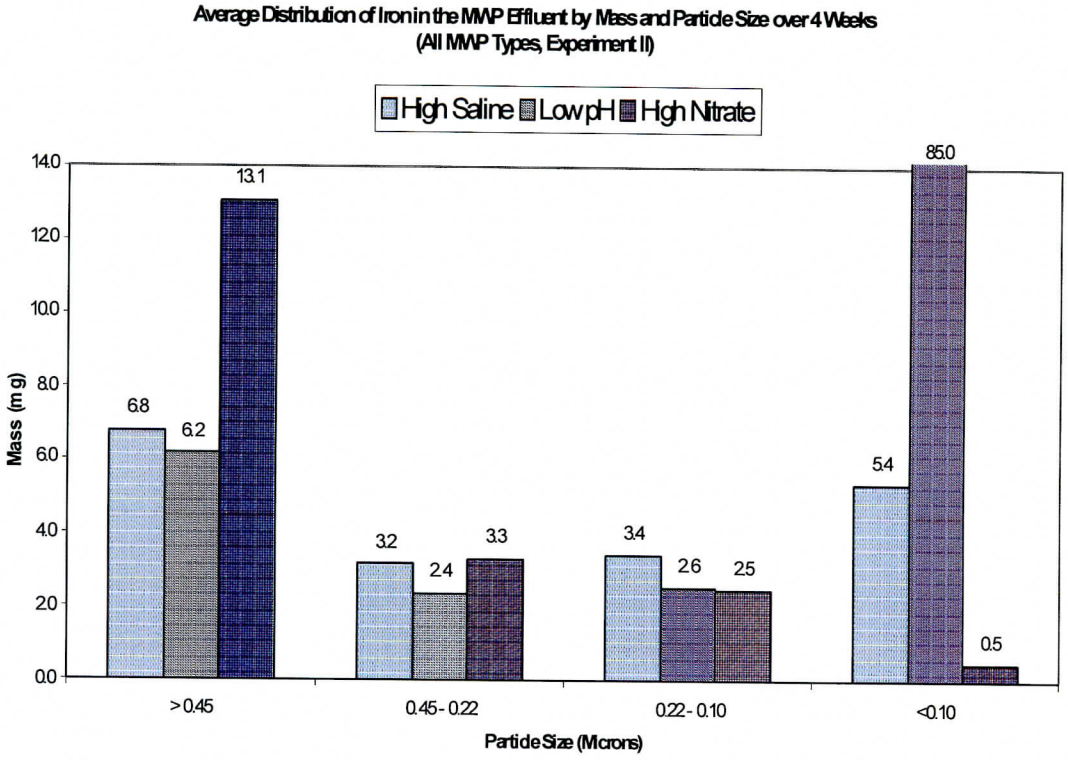

Fig. 21. Average Distribution of Iron in the MWP Effluent by Mass and Particle size over 4 weeks (All MWP Types, EXP II). See legend in Fig. 18 for calculation details.

4.3 Characterization of Transported Minerals

Selected filters were forwarded to the Nevada Bureau of Mines and Geology at the University of Nevada Reno for X-ray Diffraction (XRD) analysis to identify mineral components. The most important difference in the formation of these minerals is the availability of oxygen to iron, the effective concentration (activity) of water, and the kinetics of nucleation. The ratio of oxygen to iron in hematite and goethite is 1.50 where as in magnetite it is 1.33. Higher activity of water, e.g. with low concentrations of dissolved solutes, favors goethite over hematite. However, the thermodynamic stabilities of these two minerals, in the presence of pure water, are so close that which mineral actually begins to form typically depends on the nature of the substrates upon which they begin to grow. Once started, that mineral will generally persist, even though it may not be the most stable.

Table 10: XRD results of solids collected on filters. Data source: DID#, 034JC.003.

FN-25-HS-HN-015A	A poorly crystalline material containing magnetite ($FeFe_2O_4$).
FI-25-LPH-012B	A poorly crystalline material containing lepidiocrocite (FeO(OH)).
BI-25-HS-HN-014A	A poorly crystalline material containing magnetite ($FeFe_2O_4$).
BN-25-C-HS-001B	A poorly crystalline material containing iron oxide ($FeFe_2O_4$). This is similar to BI-25-LPH-HS-014A, but the highest intensity peak at ~34.5° 2θ is slightly offset from the coresponding magnetite peak
BI-25-C-002A:	A poorly crystalline material containing magnetite ($FeFe_2O_4$) and goethite (FeO(OH)).
FI-25-C-004A	Contains goethite (FeO(OH)), lepidiocrocite (FeO(OH)), and maghemite-C (Fe_2O_3).
FN-25-LPH-011A	Contains goethite (FeO(OH)), lepidiocrocite (FeO(OH)), magnetite ($FeFe_2O_4$) and possible sodium sulfate hydrate ($Na_2S_2O_6 \cdot 2H_2O$).
FN-25-HS-007A	Contains goethite (FeO(OH)) and lepidiocrocite (FeO(OH)).
BI-25-HS-HN-014A	Contains goethite (FeO(OH)) and kogarkoite (Na_3FSO_4).
BN-25-HS-005B	Contains goethite (FeO(OH)) and iron oxide hydrate ($Fe_2O_3 \cdot H_2O$).
BN-25-C-001B	Contains goethite (FeO(OH)), lepidiocrocite (FeO(OH)), magnetite ($FeFe_2O_4$) and possible magnesium chloride hydroxide hydrate ($Mg_3(OH)_5Cl \cdot 4H_2O$).
BN-25-HS-HN-013B	Contains goethite (FeO(OH)). At 20.66° and 29.87° 2θ are two unidentifiable peaks
BN-25-LPH-009B	Contains goethite (FeO(OH)) and magnetite ($FeFe_2O_4$). This sample was collected from liquid that drained from the continer. This liquid was air dried before sampling
BI-25-LPH-010A	Contains maghemite-C (Fe_2O_3) and possible magnesium chloride hydroxide hydrate ($Mg_3(OH)_5Cl \cdot 4H_2O$).

Particle Size Distribution: Particle sizes of the filtered solids were estimated by inspecting select filters with a scanning electron microscope (Joel JSM-5600, Joel Inc., Peabody, MA). This visual inspection revealed a range of particles sizes and what appear to be conglomerates of particles (Figs. 22 and 23). A scan of the X-rays produced from the sample when excited by the electron beam confirmed that we were interpreting the image correctly. For example, when analyzing what appear to be iron oxide particles, the EDS spectra contained peaks at ~6.41 and 7.05 keV which are energies associated with iron atoms. Conversely, the spectra for the background material contained no iron peaks but a carbon (Teflon) peak at ~0.22 keV. From the various SEM images, we conclude that individual particles generally range from about 0.2 - 0.8 microns in diameter and that larger conglomerates up to several microns in diameter are also present. Interestingly, despite having first passed through both 0.45 and 0.22 μm filters, most of the particles on the 0.1 μm filters appear to be larger than 0.22 μm in diameter. It is possible that the vacuum assisted filtration forced larger particles through the filters or that what appear to be individual particles are actually conglomerates, perhaps forming post-filtration.

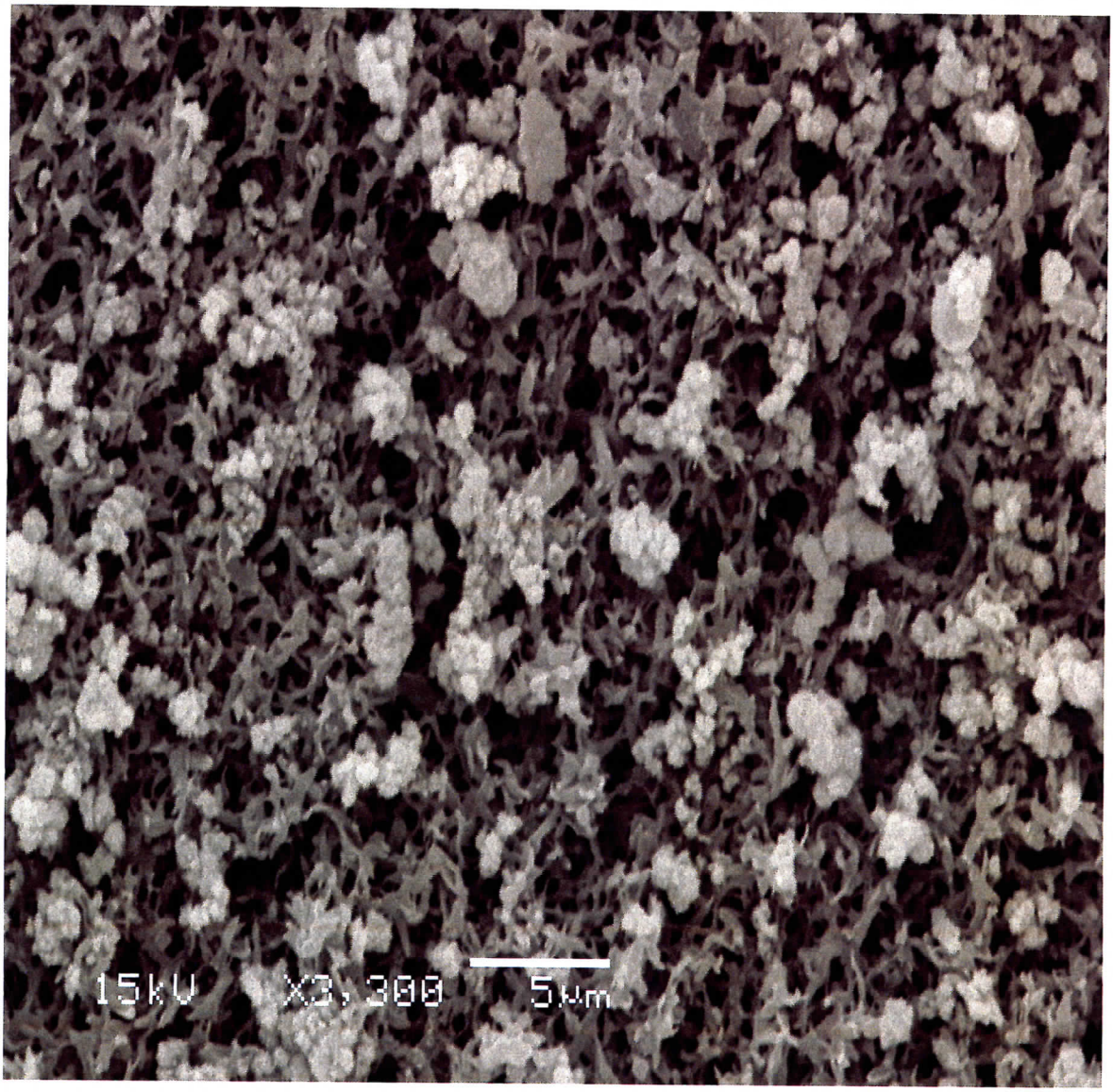

Figure 22: 300 times SEM Image magnification of filtered solids on 0.45 um filter size. Non-Q, for corroborative use only.

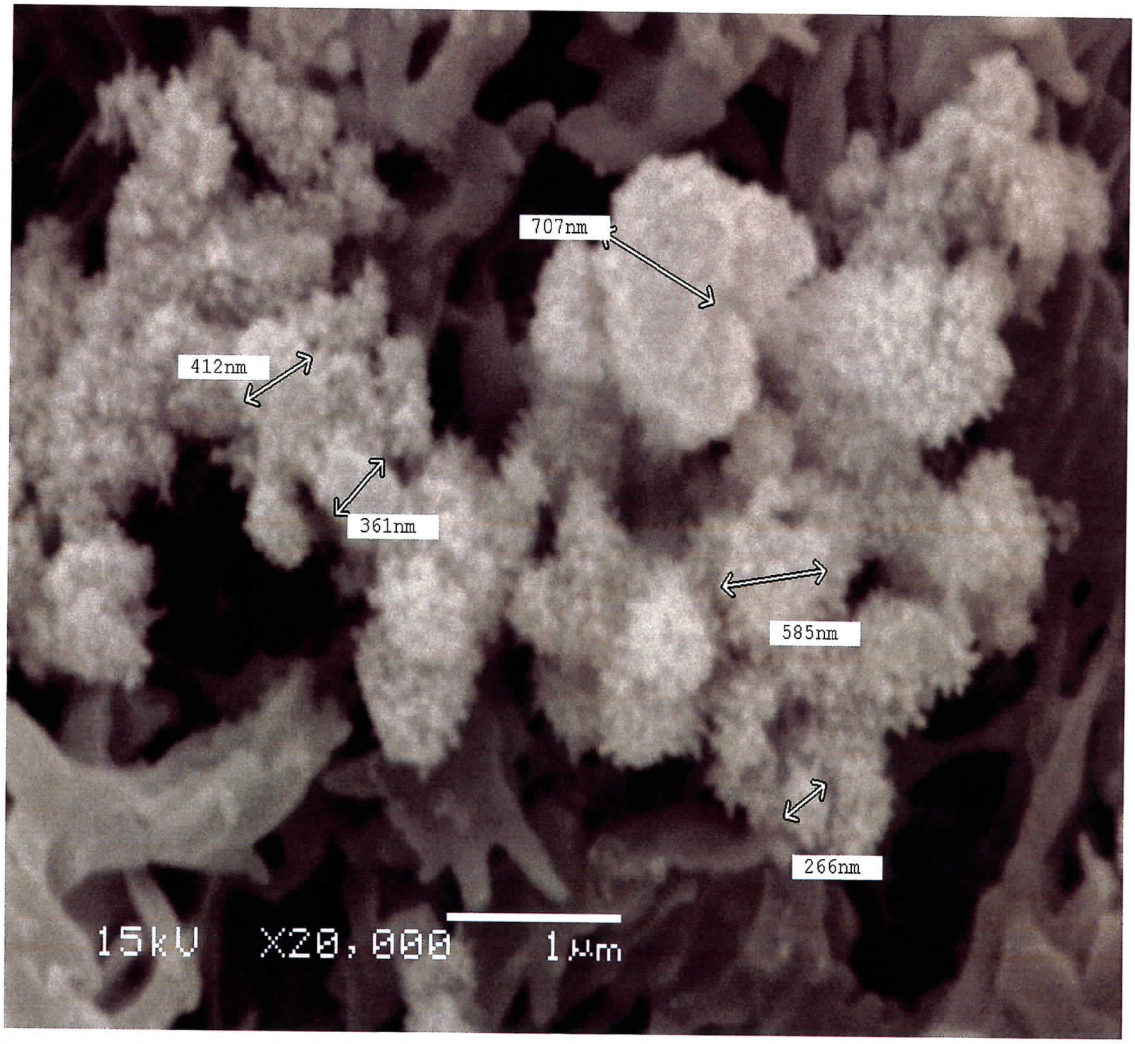

Figure 23: 20,000 times SEM Image magnification of filtered solids on 0.45 um filter size. Non-Q, for corroborative use only.

In summary, through X-Ray Diffraction and Scanning Electron Microscopy studies of the solids in the MWP effluent, we discovered that secondary minerals, such as goethite, lepidocrocite and magnetite were prevalent. Particle analyses revealed that individual particles generally range from about 0.2 to 0.8 μm in diameter are also present.

4.4 pH, conductivity, and dissolved oxygen in MWP effluent

Effluents from the MWP were monitored for changes in pH, conductivity, and dissolved oxygen on a weekly basis. Dissolved oxygen (DO) is an important factor in the corrosion process. In our study, DO ranged between about 2.5 and 5.5 ppm throughout the experiments. The starting (influent) DO concentrations were similar for experiments I and II. The DO values for J-13, low pH, high saline, and high nitrate were 5.3, 4.2, 3.9, and 3.7 ppm, respectively. In general, J-13 had the highest DO, followed by low pH, high nitrate, and high saline (Fig. 24). In experiment I, there appears to be a drop in DO after passing through the MWP for the high salt solutions, however this was not apparent in experiment II. There was a general increase in DO in the effluent for the low pH solution over the course of the experiments (Fig. 25).

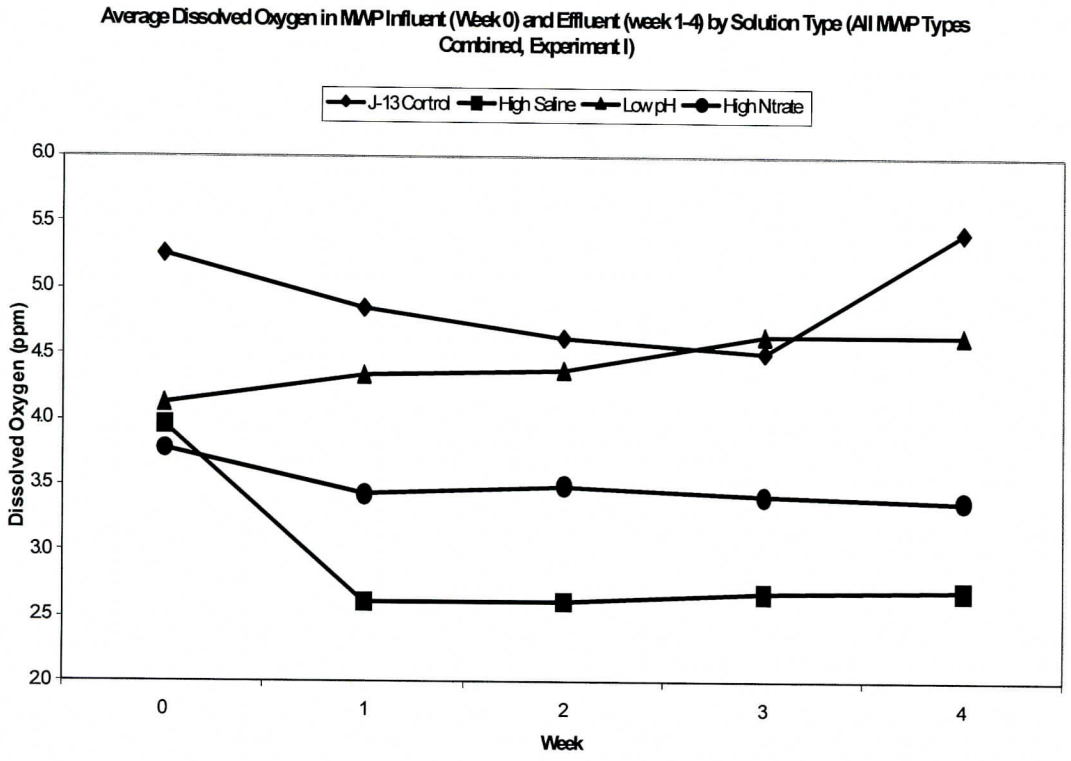

Fig.24. Average Dissolved Oxygen in MWP Inflow (Week 0) and Effluent (Week1-4) By Solution Types (All MWP Types Combined, EXPI). ; Data source: DID#034JC.001 and .034JC.007.

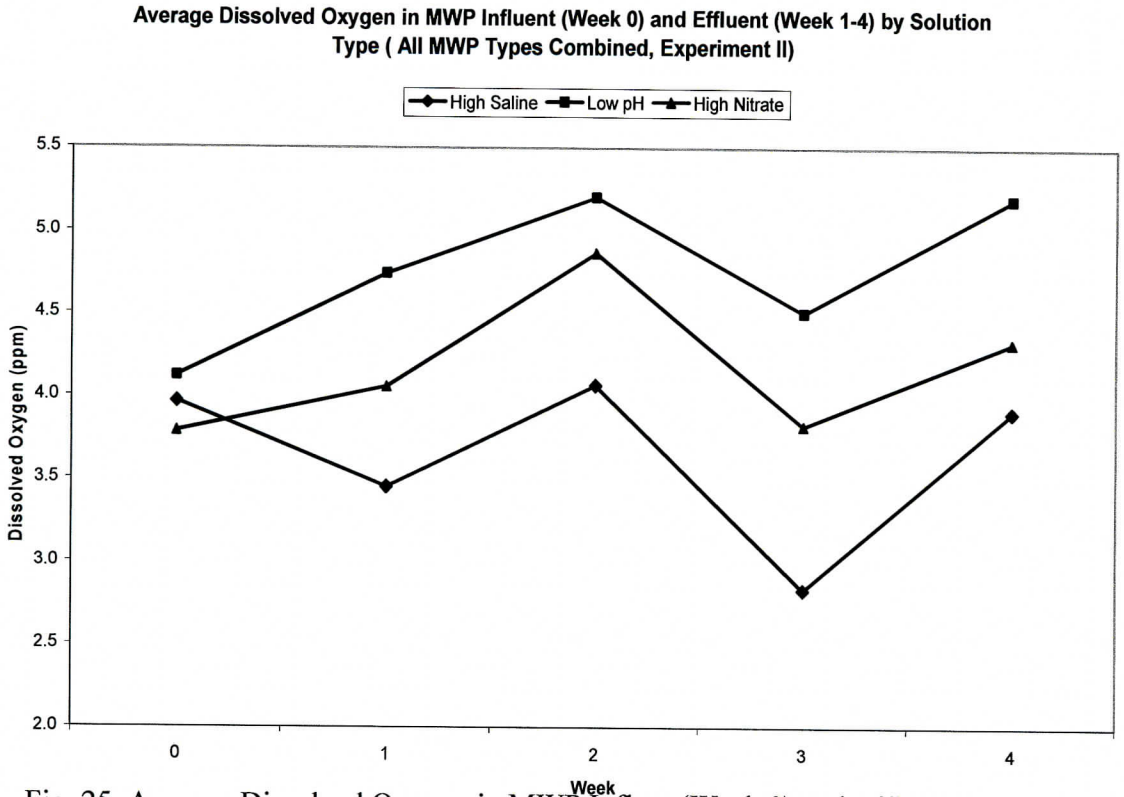

Fig. 25. Average Dissolved Oxygen in MWP Inflow (Week 0) and Effluent (Week1-4) By Solution Types (All MWP Types Combined, EXPII). Data source: DID#034JC.005 and .034JC.007.

For the J-13 groundwater, the average pH for the combined models (bathtub no shot, bathtub with shot, flow-through no shot, and flow-through with shot) rose from about 7.8 at the start of the experiment to about 8.6 by the end of week 2 where it remained relatively constant (Figs. 26 and 27). pH values for the high saline and high nitrate solutions were nearly identical throughout the experiments. The solutions started at a pH of ~9.2, dropped slightly to ~9.0 by week 1, and then gradually increased to about 9.7 by week 4. The trend was the same regardless of MWP type. The low pH solution had a beginning pH of 2.1, rose to ~4.8 by week 1, then decreased to between 3.7 and 4.2. Again, there was little difference between MWP configurations.

Conductivity varied greatly depending on the solution (Figs. 28 and 29). For the J-13 control solution, conductivity varied between 260 and 592 μ-Sm. The Low pH solution had readings of 1366 through 2320 μSm. Both the High Saline and High Nitrate solutions had readings between 70 and 112 mSm.

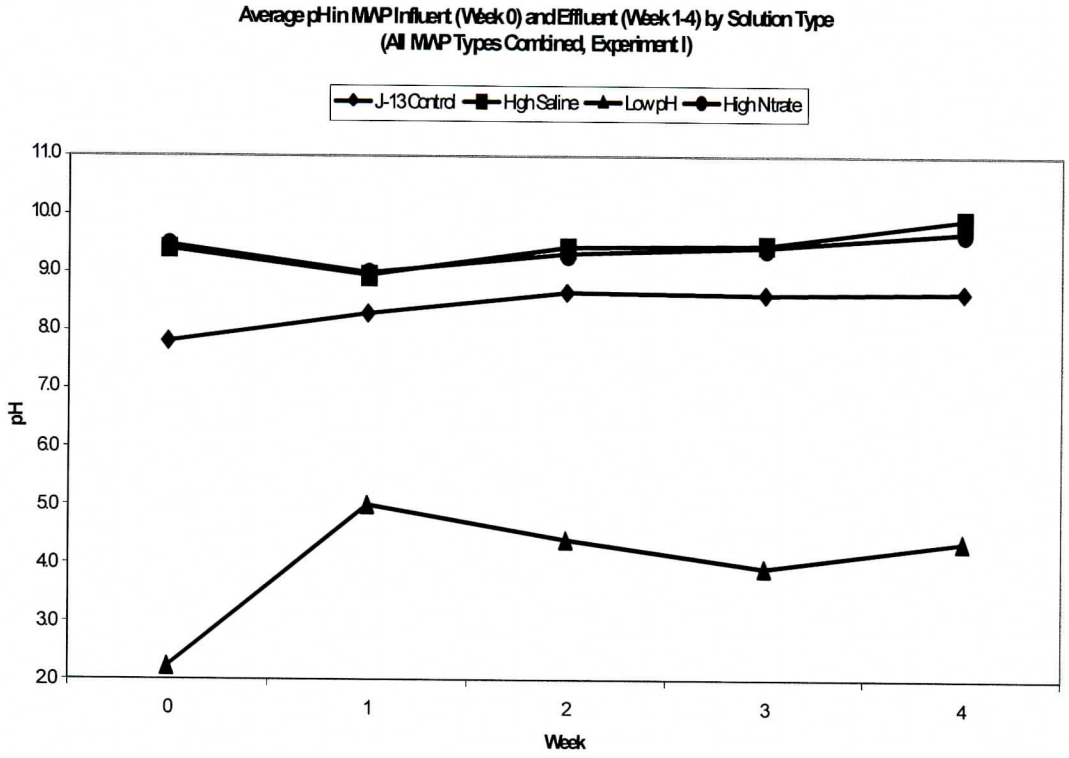

Fig. 26. Average pH in MWP Inflow (Week 0) and Effluent (Week1-4) By Solution Types (All MWP Types Combined, EXP I). Data source: DID#034JC.001 and .034JC.007.

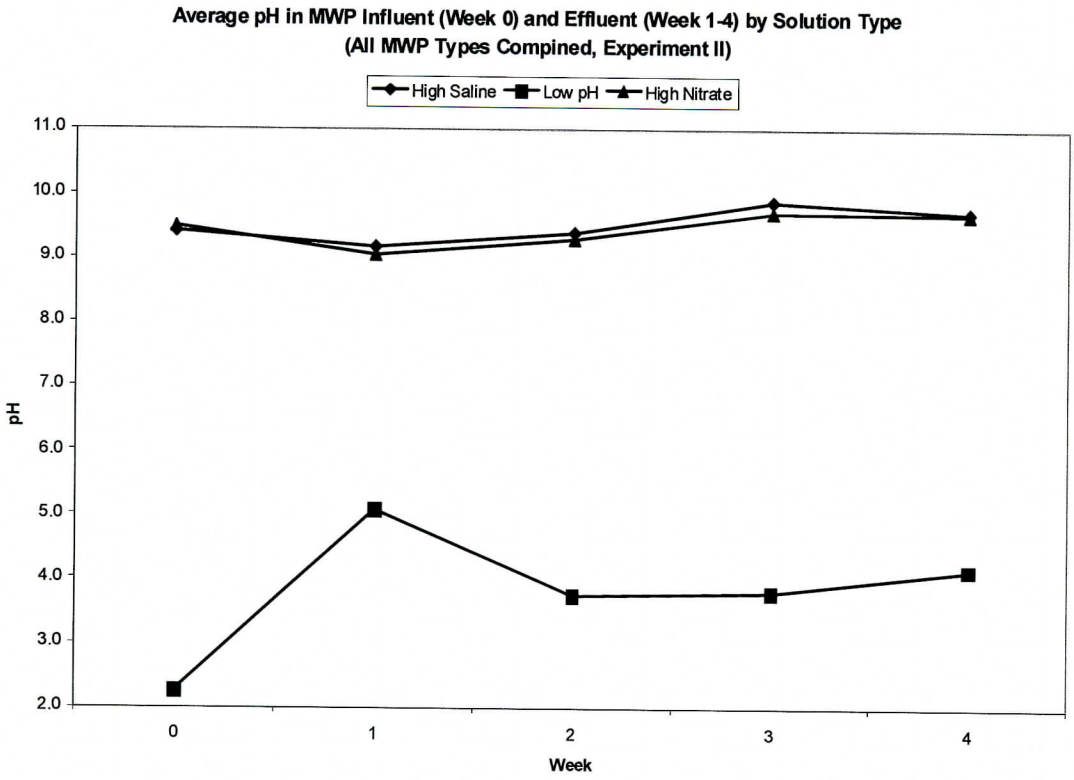

Fig. 27. Average pH in MWP Inflow (Week 0) and Effluent (Week1-4) By Solution Types (All MWP Types Combined, EXP II). Data source: DID#034JC.005 and .034JC.007.

During first week of the experiment TDS of the effluent decreased from original values of about 2500 mg/L to about 750 and remained low for the duration of the experiment. The mass of solids transported out of the MWP was greatest during the first week. Subsequently, the average mass of solids in the effluent dropped steadily until weeks 3 and 4 when there was only about 80% of the mass of the first week. Although the rate of solid transport slowed down, the pH did not go down, perhaps an indicator of a H^+ sink in the MWP. The TDS measurement of the effluent solutions reveals a rapid drop in TDS concentration to about ¼ of the concentration of the first week. The TDS remained contant the rest of the experiment. The hypothesis presented here assumes direct involvement of H^+ in production of solid corrosion products.

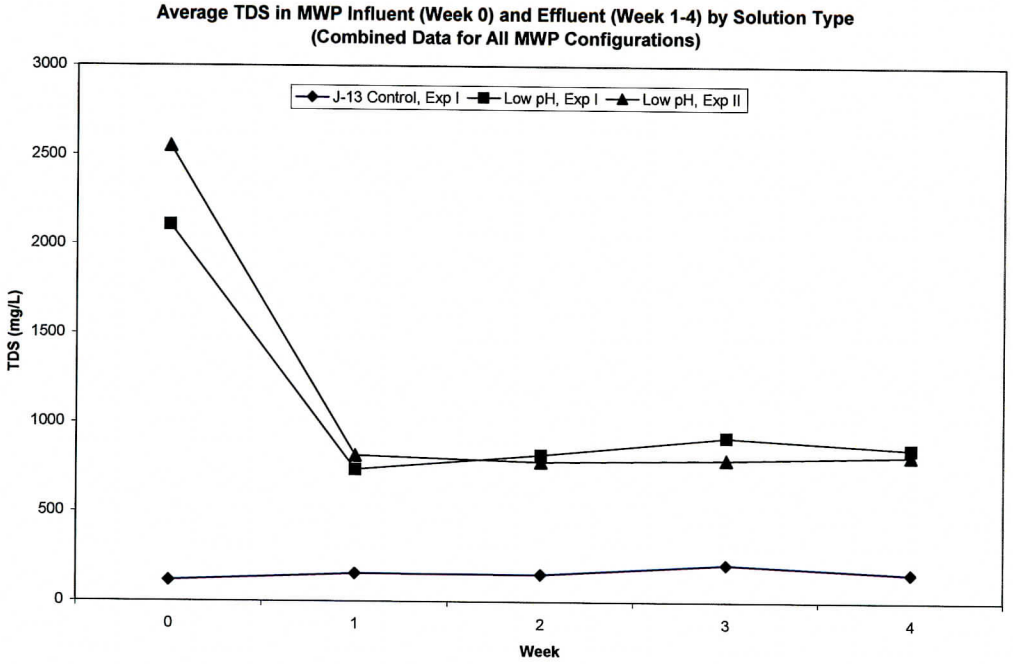

Fig. 28. Average TDS in MWP Inflow (Week 0) and Effluent (Week1-4) By Solution Types (All MWP Types Combined, EXP I and II). Data source: DID#034JC.001, 034JC.005, and .034JC.007.

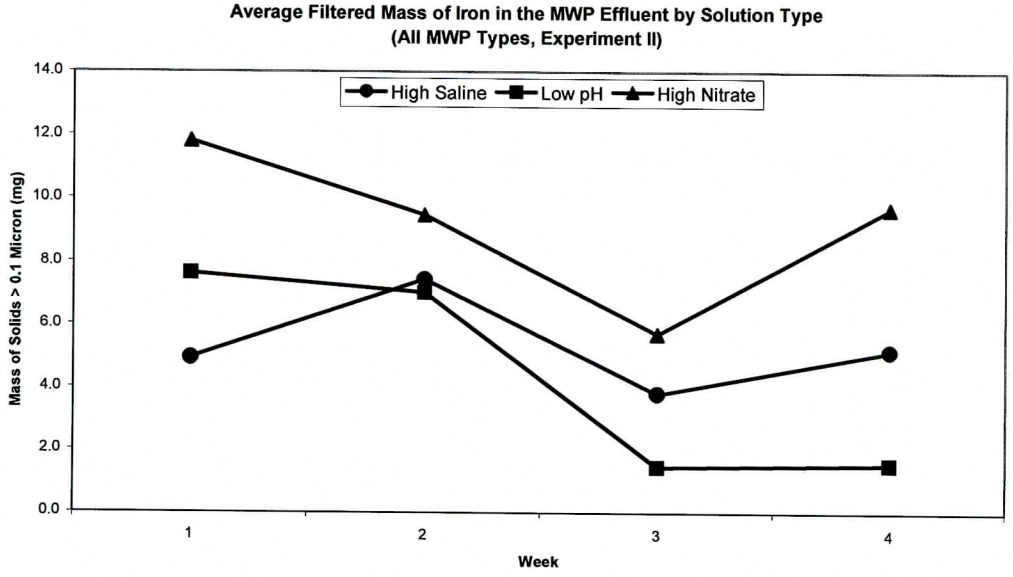

Fig. 29. Average Filtered Mass in MWP Effluent (Week1-4) By Solution Types (All MWP Types Combined, EXPII) DID#034JC.001, 034JC.005, and .034JC.007

4.5 Corrosion Processes in MWP

Corrosion of iron initiated by electrochmical reaction given by Brad and Faulkner (1980)

$Fe \longrightarrow Fe^{2+} + 2e^{-}$ E^0=-0.409V

Iron (III) ions could now form by electrochemical oxidation of dissolved Fe(II)
$Fe^{2+} \longrightarrow Fe^{3+} + e^{-}$ E^0=+0.770V

Cotton and Wilkinson present the overall oxidation of Iron(II) to iron(III) as;

$4Fe^{2+} + O_2 + 4H^{+}$ ---->$4Fe^{3+} + 2H_2O$ E^0=+0.460V

Oxidation of Fe(II) to Fe(III) in neutral and natural waters by molecular oxygen could be an ionic reaction between FeOH+ and HO_2^{-}, however, details of such reactions are uncertain. Other common oxidants in solution like NO_3^{-} and NO_2^{-} could oxidize Fe(II) to formation of a brown nitrosyl ion $[FeNO(H_2O)_5]^{2+}$ in the follwing reaction:

$3Fe^{2+} + NO_3^{-} + 4H^{+}$ ---->$3Fe^{3+} + 2H_2O$

Oldfield and Sutton discuss sequential hydrolysis reactions to form $Fe(OH)^{+}$ and $Fe(OH)_2$.

$Fe^{2+} + H_2O$ ---->$Fe(OH)^{+} + H^{+}$

$Fe(OH)_2(s)$ ---->$Fe^{2+} + 2OH^{-}$

Kolar and King reported O_2 oxidation of Fe(II) from biotite

Fe^{2+}(biotite) ---→ Fe^{2+}(aq)

4 Fe^{2+}(aq) + O_2 + $2H_2O$ ---->4 Fe^{3+} (aq) + $4OH^{-}$ (Highly pH dependent)

Fe^{3+} (aq)----→ Fe^{3+} (s)

Fe^{2+} (aq)----→ Fe^{2+} (s)

Iron (II) ion is a strong Lewis base that could react with oxygen to produce superoxide radical ion (O_2^{-}) and/or its conjugated hydroperoxyl radical (HO_2^{-}; pKa =4.8) which in turn forms H_2O_2. Rate of H_2O_2 formation in these pathways depend on pH, dissolved metal concentration and oxygen concentrations.

$H^{+} + HO_2^{\cdot} + Fe^{2+}$ ------> $H_2O_2 + Fe^{3+}$ pH<4.8, k = 1.2 x 10^6 $M^{-1}s^{-1}$

$HO_2^{\cdot} + Fe^{3+}$ ------→ $O_2 + Fe^{2+} + H^{+}$ pH<4.8, k < 10^4 $M^{-1}s^{-1}$

$2H^+ + O_2^{\cdot-} + Fe^{2+}$ ------> $H_2O_2 + Fe^{3+}$ pH>4.8, k = 1.2 x 10^7 $M^{-1}s^{-1}$

$O_2^{\cdot-} + Fe^{3+}$ ------→ $O_2 + Fe^{2+}$ pH>4.8, k = 1.5 x 10^8 $M^{-1}s^{-1}$

In natural waters, the reaction of metals and H_2O_2 is responsible for redox cycling of metals. These reactions are even more important at night (absence of UV light from sun for photoreduction reactions). Wilson et al., studied the relative importance of dissolved organic carbon pathways versus pathways involving metal-redox reactions in controlling H_2O_2 concentrations in thermal springs. They concluded that in waters where concentration of dissolved iron concentration exceeds the concentration of dissolved organic carbon, chemical reactions with reduced iron or iron-organic complexes may be important in H_2O_2 formation.

In section 4.3, Table 10 summarizes the XRD analysis of solid materials transported from (and existing inside) the MWP. In general, the dynamic inflow of water resulted in formation of mostly iron oxyhydroxide crystalline materials. It appears formation of crystalline materials is under kinetic rather than thermodynamic control. Figures 16 and 17 show the time-lapse photography of corrosion processes inside of a glass wall MWP. Formation of light brown, green, black and reddish colored corrosion products are evident in this process.

In the following we suggest a mechanism for formation of these products based on the literature search and experimental results at the low temperature regime:

Fe^0 ---------> $Fe^{2+} + 2e^-$ (1)

$Fe^0 + 2\ H_2O$ ---->$Fe^{2+} + H_2 + 2OH^-$ (2)

Fe^{2+} ---->$Fe^{3+} + e^-$ (3)

$Fe^{2+} + H_2O$ ---->$Fe(OH)^+ + H^+$ (4)

$Fe(OH)^+ + OH^-$ --------> $Fe(OH)_{2\ (s)}$ (5)

$Fe(OH)_{2\ (s)}$ --------> $FeO(OH) + H^+ + e^-$ (6)

$Fe^{2+} + Fe^{3+} + Fe(OH)_2$ s --------> $[Fe_2^{2+}\ Fe^{3+}\ O_x(OH)_y]^{(7-2x-y)}$ and/or $[Fe^{2+}\ Fe^{3+}\ O_x(OH)_y]^{(5-2x-y)}$ (Green Rust Complexes) (7)

$2[Fe_2^{2+}\ Fe^{3+}\ O_2(OH)_2]^{(1+)} + O_2^-$------>$2\ Fe_3O_{4\ (s)} + 2H_2O$ (8)

5. Conclusion

1) In most cases exit holes were clogged with corrosion products that have higher molar volume than iron. This process will reduce void volume inside the MWP available to incoming water and decreasing the probability of criticality. However, plugged waste packages could have higher probability of bottom failure. An addition of a skirt could divert water from hanging at the bottom of waste packages.
2) Average concentration of solids leaving the MWP was 20.6 mg/L. High salinity of incoming solution increases solid transport out of MWP. Low pH increases transport of total iron (dissolved and solid corrosion products) out of MWP.
3) Most corrosion products are goethite, lepidocrocite, magnetite, and maghemite, and amorphous iron oxyhydroxides. In a dynamic system it appears kinetic control plays a more important role than thermodynamics.

6. References

Brad A.J. and L.R. Faulkner, Electrochmical Methods. Fundamentals and Applications. John Wiely & Sons, New York, NY, 1980, pp. 91-92 and 699-702.

Cotton F.A., G. Wilkinson, Advanced Inorganic Chemistry, 5th Ed., John Wiley & Sons, New York, NY, 1988, pp. 679-755.

CRWMS M&O 1998. *"Unsaturated Zone Hydrology Model."* Chapter 2 of Total System Performance Assessment-Viability Assessment (TSPA-VA) Analyses Technical Basis Document. B00000000-01717-4301-00002 REV 01. Las Vegas, NV.

RWMS M&O 1999. *Waste Package Materials Properties*. Rev 00. BBA000000-01717-0210-00017, REV 00. Las Vegas, Nevada.

CRWMS M&O 2000a. *Data Qualification Report: Composition of J-13 Well Water for Use on the Yucca Mountain Project.* TDR-NBS-HS-000003 REV 00. Las Vegas, Nevada

CRWMS M&O 2000b. Total System Performance Assessment for Site Recommendation. TDR-WIS-PA-000001 REV 00 ICN 01. Las Vegas Nevada. MOL. 20001220.0045.

CRWMS M&O 2000c. EQ6 Calculation for Chemical Degradation of PU-Ceramic Waste Packages: Effects of Updated Waste Package Design and Rates. CAL-EDC-MD-000009 REV 00, Las Vegas, NV

Gu B., T.J. Pheleps, L.Liang, M.J. Dickey, Y. Roh, B.L. Kinsall, A.V. Palumbo, and G.K. Jacobs, " Biogeochemical Dynamics in Zero-Valence Iron Columns: Implications

for Permeable Reactive Barriers", Environmental Science and Technology, 33, 2170-2177, 1999.

IPLV-012 Measurement of total dissolved solids, conductivity, alkalinity and pH in water samples, Rev. 1 UCCSN Implementing Procedure, 2002.

IPLV-046 Operation of an X-Ray Diffractometer. Rev. 0. UCCSN Implementing Procedure, 2001.

IPLV-053 Determination of flow rate using the Carter Cassette Pump, Rev. 0. UCCSN Implementing Procedure, 2002.

IPLV-056 Measurement of dissolved oxygen in water samples, Rev. 0. UCCSN Implementing Procedure, 2002.

Kimura M., T. Suzuki, G. Shigesato, H. Kihira, and S. Suzuki.,"Fe(O,OH) Network structure of rust formed on weathering steel", Surface and Interface Analysis, Vol35, Issue1, pages 66-71.2003

Pitts Lynn F. and J.K. St. Joseph, "INCHTUTHIL The Roman Legionary Fortress Excavations 1952-1965", Chapters 3 and 28. Britannia Monograph Series No.6, Published by the Society for the Promotion of Roman Studies, 31-34 Garden Square, London, WC1 OPP. 1985

Roh Y., S.Y.Lee, and M.P.Elless " Characterization of Corrosion Products in the Permeable Reactive Barriers", Environmental Geology, 40 (1-2) December 2000.

Trefz J., M. Schweinsberg, T. Reier.: Systematic investigation on the corrosion of iron under conditions relevant to storage of nuclear waste. Materials and Corrosion, 1996, **47**, 475.

Rosenberg N. D., K.G. Knauss, M.J. Dibley,: Evaporation of J-13 Water: Laboratory Experiments and Geochemical Modeling, DC#23869, August 13, 1999.

Wilson, C. L.; Hinman, N. W.; Cooper, W. J.; Brown, C. F., "Hydrogen Peroxide Cycling in Surface Geothermal Waters of Yellowstone National Park ", Environmental Science and Technology, 34(13); 2655-2662, 2000.